UNIVERSITY *of the*
WESTERN CAPE

Faculty of Natural Sciences
Department of Physics and Astronomy

Radon exhalation studies for applications in low background environments.

Supervisor:

Prof R. Lindsay

Co-Supervisor:

Prof S. Triambak

Candidate:

Goitseona. J Ramonnye

A thesis to be submitted in achievement of the degree of Masters of Sciences in Physics.

DECLARATION

I, the undersigned, hereby declare that the work contained in this thesis is my own original work and that I have not previously in its entirely or in part submitted it at any other university for a degree.

Goitseona Johanna Ramonnye

Signature : .....

Date : .....

Prof R Lindsay

Director Nanoscience Platform

Department of Physics

University of the Western Cape

Signature : .....

Date : .....

Prof S Triambak

NRF/DST SARChI Chair

Department of Physics

University of the Western Cape

Signature : .....

Date : .....

ACKNOWLEDGEMENTS

I am highly indebted to both my supervisors, namely Professor Robert Lindsay and Professor Smarajit Triambak, for their continuous guidance and support from the beginning of my academic journey that has lead to completion of the project. It is with greatness that both my supervisors have invested their time and worked tirelessly to impart valuable knowledge which has laid an enormous foundation for my research growth. Your scholarly guidance has been immeasurable in shining a light of knowledge required for this work. Your supervision, availability and devotion for your time has allowed an extensive understanding and stimulated a deeper interest in the study of double beta decay and connection that to radon emanation measurements from different materials.

I am grateful to the Department of Physics at the University of the Western Cape for making provision and allowing access to perform laboratory experiments that has enabled me to use the equipment necessary for this project. I extend my appreciation to the National Research Foundation for fulfilling its mandate in promoting and supporting many young individuals like myself to pursue our studies in research as well as facilitating human resource development. Thank you for granting me the opportunity to fund my studies. I can confidently say that the experience of working on this project has been enriching.

Many thanks to the collaboration provided by the nEXO people through the low level radon sensitivity project, particularly Jacques Farine. The partnership you have provided gave invaluable input to my project and an opportunity to be involved in a world-class experiment towards the search neutrinoless double beta decay. Thank you.

The opportunity to embark on this study would not been possible without Professor Robert Lindsay's tireless motivation and resilience in convincing the community to accept me as a student that meets the criteria for an MSc despite my background. My earnest appreciation goes to those that granted me an approval to pursue this study.

A special thanks to my friends, Lindiwe Sikhakhane, Sarah Khumalo, Tshiamo Setuke, Sipokazi Panya Panya, that offered me constant encouragement and support that has carried me thus far. Your words of encouragement has nurtured my determination.

To my school teachers and mentors, thank you for laying a foundation, for instilling an imagination that inspired to become a person that will add value into the community and aspire for change. A profound thanks to Mr David Ryan for dedicating his life to volunteer in teaching rural schools in which I was able

improve my mathematics marks and be able to enroll for a qualification in science. You have laid a solid rock that has afforded me my dreams, I owe this to you.

To my loving parents, my father Sipho Abbysia Ramonnye and my mother Malekone Agnes Ramonnye, I exalt my heart to you for the role that you have committed your life into and endured, for the many sacrifice to secure me a better future and being the pillar of my life. To my sisters, Shanana Magoro and Lerato Ramonnye, that has led the path before me and support every chapter in my life. Thank you for your words of wisdom.

To my supportive fellow students, Sumeera Gopal, Sifiso Mngonyama and Xolisani Ngwadla, for the assistance and filling in where I needed to improve my skills. You all have made the journey smooth and short.

Finally, to my loving and supportive partner Siphesihle Mchunu, I extend my gratification to you. I am grateful that we were able to cross path at same time I embarked on this journey. You have encouraged me until the finish line. To you all, mentioned and unmentioned, I thank you immensely.
Goitseona Johanna Ramonnye

ABSTRACT

Neutrinoless double beta decay ($0\nu\beta\beta$) is a rare process that is yet to be observed. Observation of neutrinoless double beta decays would imply lepton number violation, and that the neutrino is its own antiparticle (a Majorana fermion). Understanding background contributions are important in searches for such rare nuclear processes. This thesis details the design and operation of a radon detector in the context of low-background deep-underground experiments, such as the one pursued by the nEXO neutrinoless double beta decay collaboration.

Most sensitive rare search experiments are located deep underground to shield from cosmic radiation. However, radon presents itself as a pervasive source of background in such environments. Radon is the only daughter in the uranium and thorium decay chains that is gaseous, so it has the ability to escape materials either through pores or diffusion through material. This background would potentially make any rare physics search ineffective, as the signals of interest may be clouded by background noise.

For the purpose of this project a Durridge RAD7 radon detector was used to measure charged alpha particles of radon daughters. The detector is sensitive to ^{218}Po, with the photo-diode and a radon concentration in the gas, which is determined from the measured activity. Utilization of this detector provides values of ambient radon backgrounds to sensitivity of the order mBq/m^3. Experiments were conducted at pressures below atmospheric pressure and in an argon environment to compare with normal air experiments. A mercury manometer was used to monitor the pressure.

Our measurements of a rubber sample provided by the nEXO collaboration as a test case, showed that our system of a 12 L stainless steel container that was used as a sample holder that is then linked to the RAD7, does not have the lower level of detection that is required to measure at the level needed for the nEXO exhalation measurements. Those measurements require an accuracy at the order of atoms per day. The sensitivity to the atmosphere used and the pressure was then tested with a strong source in the form of a rock from a monazite seam in a local mine that produces several hundred thoron atoms per second. This activity from this rock indicated that both the atmosphere and pressure do affect the thoron exhalation from the rock.

Contents

List of Figures

Chapter 1

Introduction

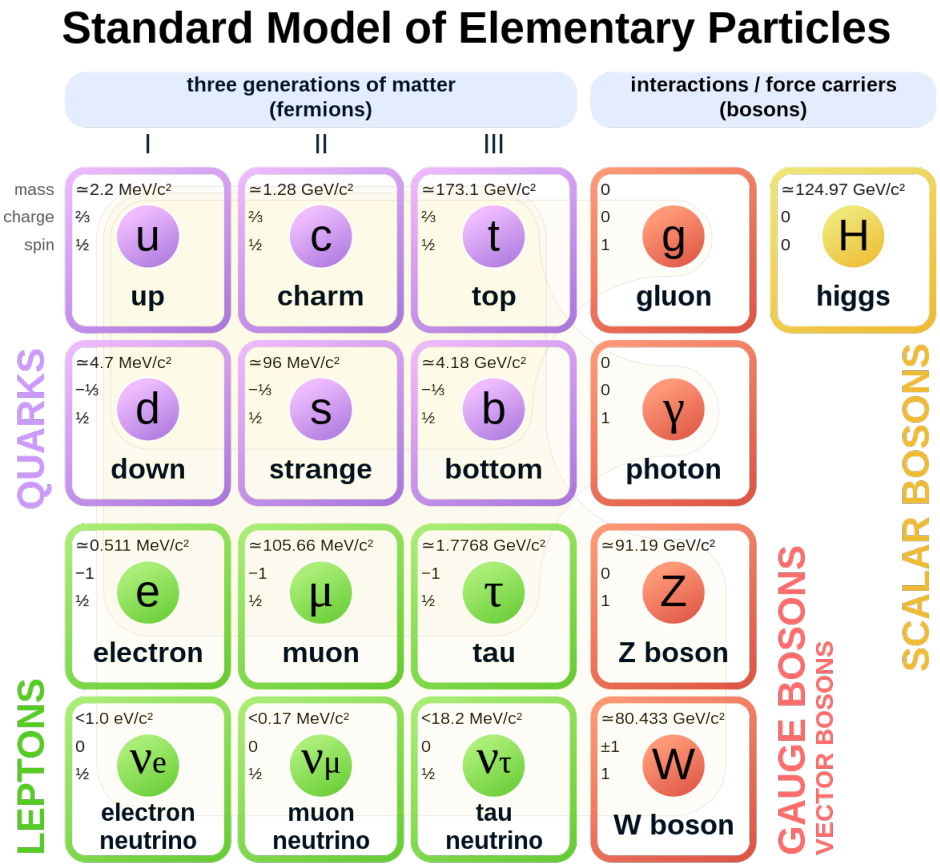

Figure 1.1: Elementary particles and their interactions, as classified in the Standard Model [1].

The emergence and development of modern physics during the 20^{th} century was a giant leap in the history of human-kind. Modern physics includes the concepts beyond Newton's laws, Maxwell's equations, and thermodynamics, which constitute "classical" physics. Such new ideas emerged after unknown forms of radiation such as X-rays, α, β and γ radioactivity [2] were observed and subatomic particles (such as the electron) were discovered. Additional breakthroughs took place through the development of the special theory of relativity, which recognized that the speed of light in vacuum ought to remain constant in all reference frames of motion, in accordance with Maxwell's equations of electromagnetism. Together with special relativity, the development of quantum mechanics to describe observed atomic phenomena, marked a consequential development in the field of modern physics.

In principle, the behavior of atoms, the periodic table of elements and their chemical behavior, as well as the spectroscopic, electrical and other physical properties are described by the laws of quantum mechanics. This extends to nuclei, nucleons, photons and other subatomic particles such as quarks and leptons, described below. Quantum mechanical theories deal with probabilities and uncertainties, and have thus far met every experimental test. For example, predictions such as those of quantum electrodynamics (QED), are some of the most precise and best checked, being accurate to better than one part per billion [2].

The most rapid development in the field occurred in the past 60 years or so, with the advent of high energy particle accelerators and sophisticated detector systems. Several new kinds of subatomic and elementary particles were discovered during this time. Simultaneously there were rapid developments in theoretical physics that successfully described the properties of these newly discovered particles. The culmination of this work resulted in the development of the Standard Model of Particle Physics [2], which classifies elementary particles and fundamental forces, as shown in Figure 1.1. The four basic forces of nature, in order of increasing strength, are the gravitational force between particles with mass, the weak force by which quarks can change their type [2], the electromagnetic force between particles with charge and the strong force between quarks. The Standard Model [3] classifies matter as quarks or leptons. Each classification consists of of six particles, which are related in pairs and have half-integral spin. Gravity is left out of this description as it is yet to be described successfully using the laws of quantum mechanics.

The other three fundamental interactions are described within the Standard Model to be mediated by the exchange of quanta, called vector gauge bosons. The Standard Model also unifies the electromagnetic and weak interactions in a manner such that a gauge symmetry renders the photon massless, with the weak interaction force carriers (gauge bosons) (W^+, W^- and Z) acquiring large masses. This is called the electroweak theory.

Nuclear physics played a critical role in the development of Standard Model, as nuclear processes involve three of the four known fundamental forces of nature, electromagnetic, strong and weak interactions. Below I describe nuclear beta decays which occur via the weak interaction, that plays a critical role in the development and study of standard electroweak theory.

1.1 Nuclear β decays

Key to our present understanding of the Standard Model are neutral leptons called neutrinos that are emitted via nuclear beta decays, among other processes. Neutrinos were previously assumed to be massless, until neutrino oscillation measurements from SNO [4] and Super KamioKande [5] proved otherwise. The masses of the neutrinos are presently unknown, yet known to be several orders of magnitude smaller than the other leptons in Figure 1.1. Although the Standard Model is successful in describing how the W bosons and other charged leptons acquire mass (through the Higgs mechanism), it fails to describe the smallness of neutrino masses.

Electron neutrinos (ν_e), and their corresponding antiparticles ($\overline{\nu}_e$) emitted in beta decays are essentially through the transformation of an up quark to a down quark and vice versa. Since neutrinos are weakly interacting particles and nuclear β decays proceed via the weak interactions, β decays are key to a better understanding of neutrino physics. There exist three β decay modes:

$$\beta^- \; decay : n \rightarrow p + e^- + \overline{\nu}_e. \tag{1.1}$$

$$\beta^+ \; decay : p \rightarrow n + e^+ + \nu_{\rm e}. \tag{1.2}$$

and electron capture decay (the process thereby changes a nuclear proton to a neutron and simultaneously cause the emission of an electron neutrino). The latter process is shown in Fig 1.2.

$$electron \; capture \; decay : p + e^- \rightarrow n + \nu_{\rm e}. \tag{1.3}$$

There are certain conservation laws associated with β decays. One of the conserved quantities is the charge. A neutron has zero charge, a proton has a charge +1 while an electron has a charge -1. Another conservation is the baryon number. A neutron (considered a baryon, as it is made up of three quarks) has a baryon

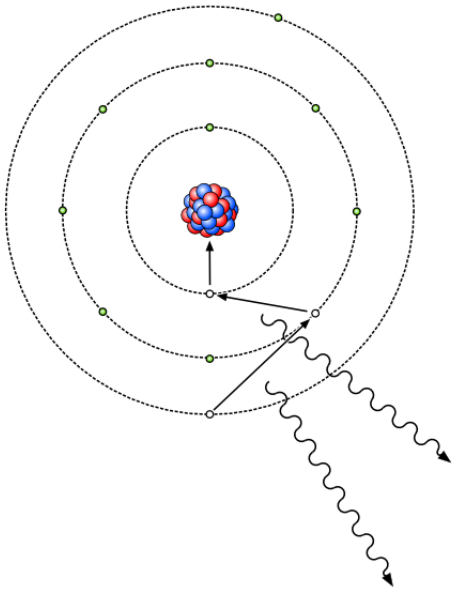

Figure 1.2: Electron capture decay.

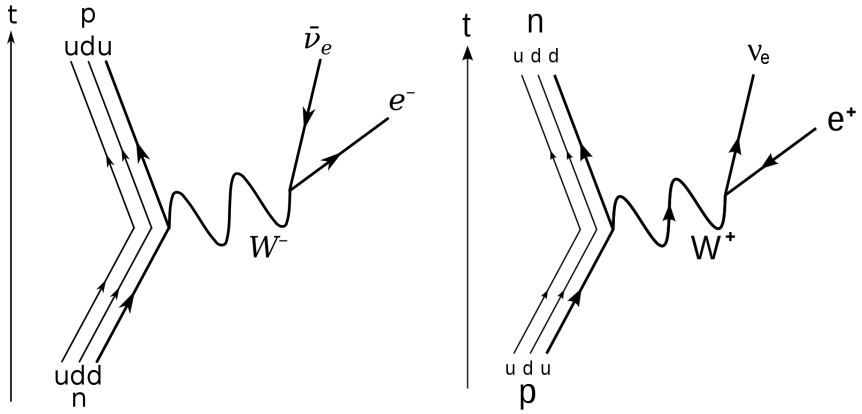

Figure 1.3: Feynman diagrams for single β^- (left) and β^+ (right) decay.

number +1, a proton (also a baryon) has a baryon number +1, while electrons and neutrinos have a baryon number 0 (they are leptons and point particles).

Lepton number is another property that is known to be conserved. A neutron and proton have no associated lepton numbers. An electron has a lepton number of +1. A positron on the other hand is its corresponding antiparticle. It therefore has a lepton number of −1. Consequently, to conserve lepton number in a β decay process, an antineutrino is emitted in β^- decay, while a neutrino is emitted in β^+ decay, as shown in Fig 1.3.

While a free neutron can undergo β^- decay, a free proton cannot β^+ decay to a heavier neutron. This

process is only possible in nuclei, where the binding energy provides the extra energy for the decay. The Q-value for a nuclear decay is the difference between the initial and final nuclear mass energies.

Consider a nuclear decay $X \rightarrow Y+D$, where D is the decay particle. According to the previous definition, the decay Q-value is:

$$Q = (m_{\mathrm{X}} - m_{\mathrm{Y}} - m_{\mathrm{D}})c^2. \tag{1.4}$$

This equals the total kinetic energy gained by the decay fragments Y and D, such that

$$Q = K_{\mathrm{Y}} + K_{\mathrm{D}}. \tag{1.5}$$

The kinetic energy of the daughter nucleus, K_{Y}, is called the recoil energy. Since the daughter nucleus is heavier than the decay particle, i.e $K_{\mathrm{Y}} << K_{\mathrm{D}}$, most of the decay energy appears in the form of kinetic energy of the decay particle.

In the case of a nuclear β decay, which was discovered around 1900, the existence of neutrinos were not yet known. If one assumes nuclei at rest to β decay, then the β energy spectrum is expected to be a sharp peak at the decay Q-value. However, it was observed that the spectrum was continuous, as shown in Fig 1.4.

Wolfgang Pauli proposed a solution in 1931 that a previously unknown and undetected massless particle

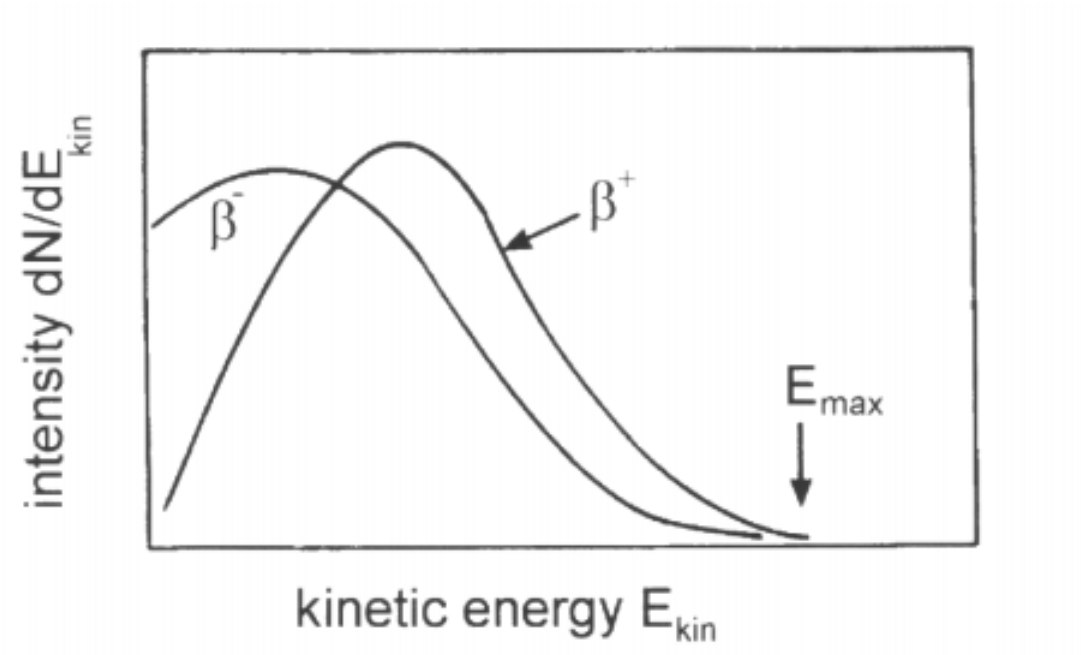

Figure 1.4: Kinetic energy spectra of electron and positron emitted in a β decay

was also emitted in the process, which shared the decay energy with the β particle. This newly postulated spin $\frac{1}{2}$ particle was later called a neutrino by Enrico Fermi. Neutrinos interact weakly with matter and were not actually detected until 1953.

The fact that neutrinos have spin $\frac{1}{2}$ means that total angular momentum is also conserved. The decay Q-value is now shared between the energies of the electron and the neutrino. This explains the continuous β energy spectrum, as the energy of the β particle can be anywhere in the range 0 to $E_{\max}$, where $E_{\max}$ corresponds to the maximum kinetic energy, Q.

1.2 Double beta decay

A nucleus in an initial state (Z, A) can also beta decay to a lighter $(Z+2, A)$ nucleus and emit two electrons and two neutrinos in its final state. This is called two-neutrino double beta decay ($2\nu\beta\beta$), and is represented by

$$(A, Z) \rightarrow (A, Z+2) + e^- + e^- + \overline{\nu}_{\mathrm{e}} + \overline{\nu}_{\mathrm{e}}. \tag{1.6}$$

In 1937, Etttore Majorana postulated the possibility of a neutrino being its own antiparticle, which would allow double β decays with the emission of no neutrinos,

$$(A, Z) \rightarrow (A, Z+2) + e^- + e^-. \tag{1.7}$$

The Feynman diagrams for these $\beta\beta$ processes are shown in Fig 1.5. The former is a second order weak interaction process and allowed by the Standard Model. The first actual laboratory observation of $2\nu\beta\beta$ decay with an estimated half life of $T^{\beta\beta}{}_{1/2}$= 1.4 $\times 10^{21}$ years was recorded during the 90's, for the ^{130}Te nucleus [6]

Unlike the two-neutrino double beta decay mode ($2\nu\beta\beta$), neutrinoless double beta decay ($0\nu\beta\beta$) only occur if neutrinos are Majorana particles. Observation of the process will imply violation of lepton number and show a direct indication or new physics, beyond the Standard Model. The possibility such $0\nu\beta\beta$ decays

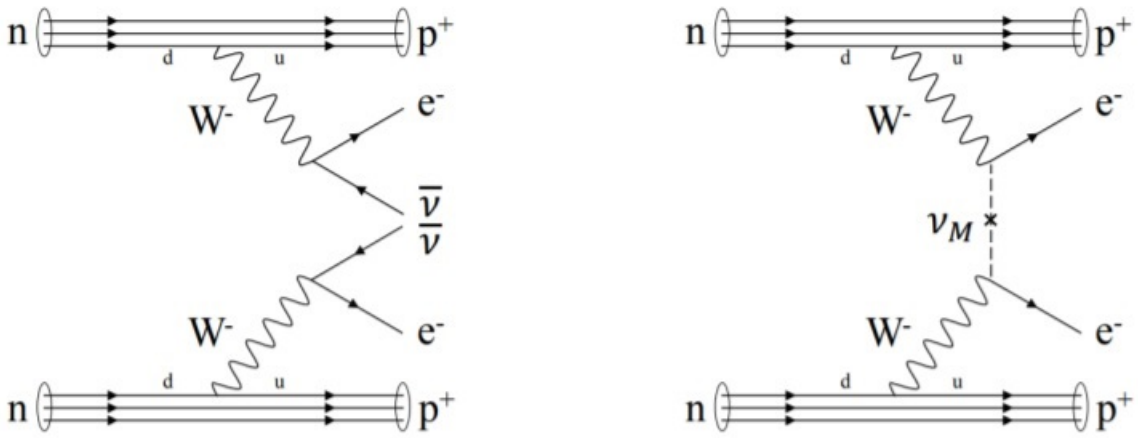

Figure 1.5: Feynman diagrams of the double beta decay (left) and the neutrinoless double beta decay (right)

exists because it is now established that neutrinos are not massless leptons, as $0\nu\beta\beta$ decays are forbidden for massless neutrinos [7].

Due to the above, many studies have been dedicated towards the search of $0\nu\beta\beta$ decays, with the goal to obtain experimental evidence of physics beyond the Standard Model [8]. Two proposed experiments are nEXO [9] and NEXT [10], which aim to have xenon time projection chambers (TPCs) enriched to $A = 136$, in liquid and gas phases, respectively. This technology will search for ^{136}Xe $0\nu\beta\beta$ decay and requires good energy resolution ($\sim 1\%$) and ultra-low background to discriminate background events that may interfere with $0\nu\beta\beta$ events of interest.

In this regard, a ^{222}Rn daughter ^{214}Bi, whose decay includes a γ-ray with an energy of 2447.7 keV is around 10 keV away from the ^{136}Xe $0\nu\beta\beta$ Q value ($Q_{\beta\beta} = 2458.07 \pm 0.31$keV). This interference is in the region of interest [11].

Other similar experiments include CUPID [12] and LEGEND [13] (are intended to search for $0\nu\beta\beta$) and LUX-ZEPLIN [14] and Darwin [15] (for dark matter).

Radon daughters deposited on the surface or searches in the bulk of detector materials have the potential to cause noticeable backgrounds within the important regions of interest. Understanding and minimizing these background signals is therefore a paramount concern in rare physics searches, in order to distinguish a real signal from internal detector backgrounds.

This brings us to the purpose of this work, which is to measure the radon emanation from materials in different environments, that may contribute to backgrounds in experiments such as the ones described above. A good knowledge of radon emanation by materials is invaluable for the eventual design and construction of such experiments that search for extremely rare processes.

1.3 Purpose of this work

Radon daughters in the decay chain of ^{238}U and ^{232}Th are found in nearly all materials at least at 1 part per 10^{20} levels. Radon is a noble gas and can escape from material and enter the surrounding environment.

This work investigates the feasibility of using a particular kind of detector (a RAD7) to perform sensitive background measurements required for rare physics experiments (such as $0\nu\beta\beta$ and dark matter). A butyl rubber sample with a known radon emanation was used for the study, together with related ancillary measurements.

This thesis also reports measurement of thoron emanation obtained from a very active rock, from the Steenkampskraal mine located in the Western Cape province of South Africa. The rock was used to check on the emanation dependence on varying external parameters such as the pressure of the gas into which the thoron was emanating.

1.4 Primordial radionuclides

There are several naturally radioactive decay chains that are present from primordial radionuclides. Backgrounds from primordial isotopes are especially pervasive in an underground environment (which is absolutely critical for searches of $0\nu\beta\beta$ or dark matter). The soil and rock placed inside the detection setup also contain varying levels of natural radioactivity.

Radionuclides, such as uranium, thorium, and potassium [16] present the largest contributions to underground radioactivity due to a combination of high relative abundance and relatively short lifetime compared to other primordial nuclides. ^{235}U, ^{238}U and ^{232}Th all alpha decay with energies in the vicinity of 2 - 7 MeV.

Contamination of U and Th on detector surfaces can produce signals from degraded alpha particles. The decay products of U and Th decays are certainly harder to shield, particularly radon [17]. Radon is a decay

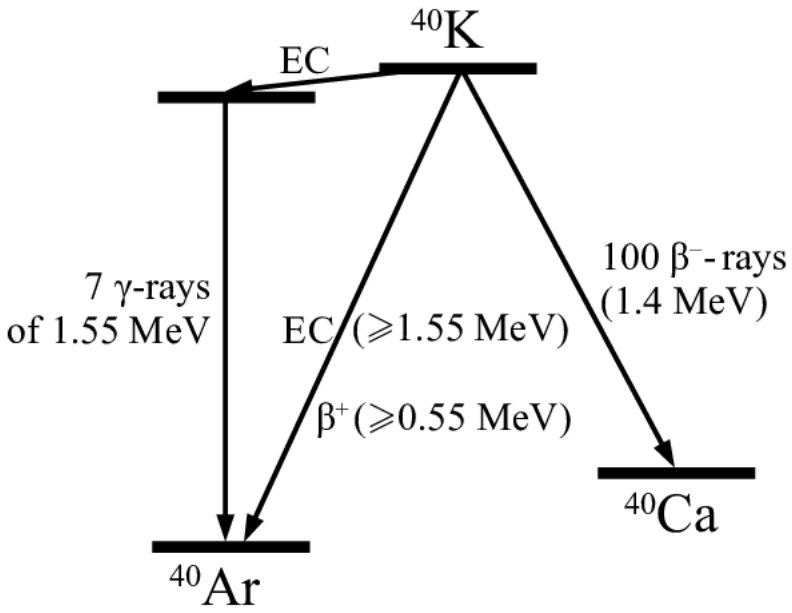

Figure 1.6: Potassium-40 undergoes three types of radioactive decay. The three different cases are that it can either decay to ^{40}Ca with emission of a beta particle and an antineutrino or it decays to ^{40}Ar by electron capture.

daughter that is hard to shield. As it is a noble gas, it does not get chemically captured or adsorbed.

As mentioned previously, for the nEXO and NEXT $0\nu\beta\beta$ experiments, most of the radiation background contributions is from ^{214}Bi (a ^{222}Rn daughter), as ^{214}Bi emits a γ-ray with an energy only 10 keV lower than the $Q_{\beta\beta}$ value. As a result, any process that contributes to a steady-state population that is only 10 keV of ^{222}Rn becomes important. Experiments that seek to monitor radon provides an understanding of the radon background level so that a maximal mitigation can be achieved.

1.5 Method to measurements and reduce radiation background.

Several techniques are used for dark matter and $0\nu\beta\beta$ decay experiments to measure and minimise background due to natural radioactivity. Radioassay is a central aspect of demonstrating the tracing of low activity present in the material.

A typical radon emanation measurement requires two counting runs, one with the sample and the other with

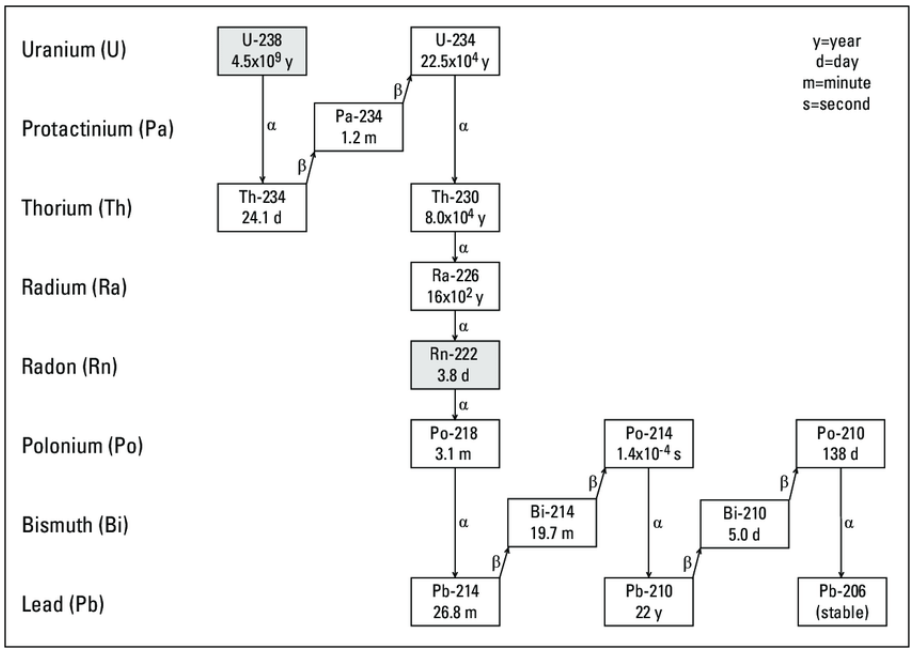

Figure 1.7: ^{238}U decay series is complex and produces alpha, beta and gamma radiation. This figure shows ^{238}U decays through a series to become a stable form of lead. Each step indicates a different nuclide and below is the length of the respective radionuclide's half life.

exactly the same configuration but no sample (blank). The results from the blank run include the counter background and are subtracted from the sample run results to produce the net emanation rate of the sample.

Neutron activation analysis (NAA) s a very sensitive method for qualitative and quantitative determination of elements based on the measurement of characteristic radiation from radionuclides formed directly or indirectly by neutron irradiation of the material, i.e. the characteristic radiation emitted in the specific decay of the unstable nuclei which are formed [18]. By knowing the trace elements, a suitable technique can be employed to reduce those elements.

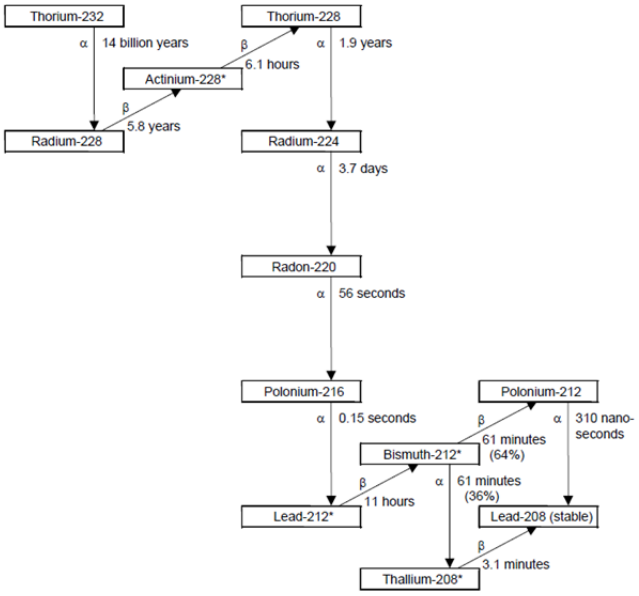

Figure 1.8: ^{232}Th decay series. The only gaseous product in the thorium decay series is thoron, which has a very short half-life (56 s). It can be used to determine ^{220}Rn as well as its parent, ^{232}Th.

Chapter 2

Methodology for Radon Emanation Measurement

In general, nearly all materials exhibit some level of radon found in the decay chain of ^{222}Rn and ^{220}Rn. Accurate measurements of radon contributions from components or materials that are used in rare physics search experiments are important to help in choosing materials that give off as small amount of radon as possible. For rare nuclear search experiment such as nEXO, the aim is to have less than 600 radon atoms in the TPC.

The initial procedure was to calibrate our detection system for radon emanation. This system has been used for several experiments of this project, but for cases where the radon levels were much higher in comparison to the needs for dark matter or $0\nu\beta\beta$ decay searches. This first experiment has been designed to investigate the radon emanation from rubber, and test the radiopurity of this material, which was received from nEXO collaborators at Laurentian University in Canada. This rubber sample has been used to test radon escape by various groups in the collaboration.

The measurements and data extracted from the experiment are compared to other experimental setups in line with nEXO collaborators involved in radon measurement. The components of the setup (as shown in Figures 2.1 and 2.2) and the operation of the experiments are elaborated in depth below.

Figure 2.1: The University of the Western Cape(UWC) radon detection setup.

2.1 RAD7 Radon detector System

An Electronic Radon Detector, the RAD7 detector, supplied by Durridge Company (USA), was used in the present work. The RAD7 (Durridge Company, Bedford, MA) is a highly versatile alpha spectroscopy instrument for radon detection and the radon concentration can be obtained in real time.

Its internal cell is a dome with volume 0.7 liter. An Ion-implanted, Planar, Silicon alpha detector is at the center of the hemisphere. The high voltage power circuit charges the inside conductor to a potential of

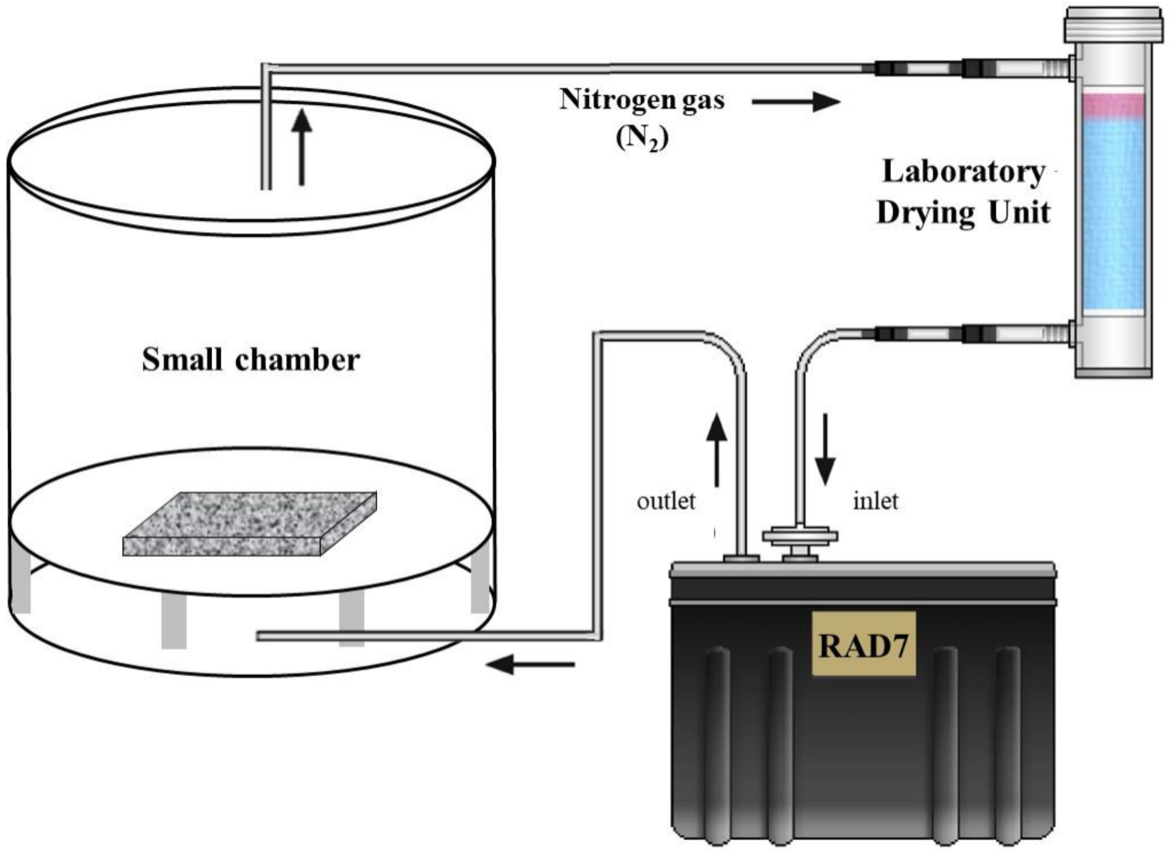

Figure 2.2: The RAD7 device for measuring radon concentration of the samples. A schematic drawing of the setup, illustrating when the system is flushed with nitrogen (using a gas cylinder).

2000 to 2500 volts, relative to the detector.

Figure 2.3 illustrates the internal structure of RAD7 (the dome in the center of the picture is the internal cell). The air is drawn into the internal cell of the RAD7 through a drying unit and filter by the internal pump. Because all the daughters of ^{222}Rn and ^{220}Rn are removed by the filter, the daughters in the internal cell of the RAD7 are from fresh decays of the ^{222}Rn and ^{220}Rn atoms in the cell.

Most of the freshly produced daughters, primarily ^{218}Po and ^{216}Po are positively charged since they lose electrons when recoiling during the radon decay. The electric field propels these positively charged particles onto the negatively charged detector. The speed of alpha particles emitted from ^{222}Rn, ^{220}Rn and their daughters is very high, hence alpha particles will not be collected on the detector by the electric field, because they lose energy rapidly by the interaction with the air in the chamber.

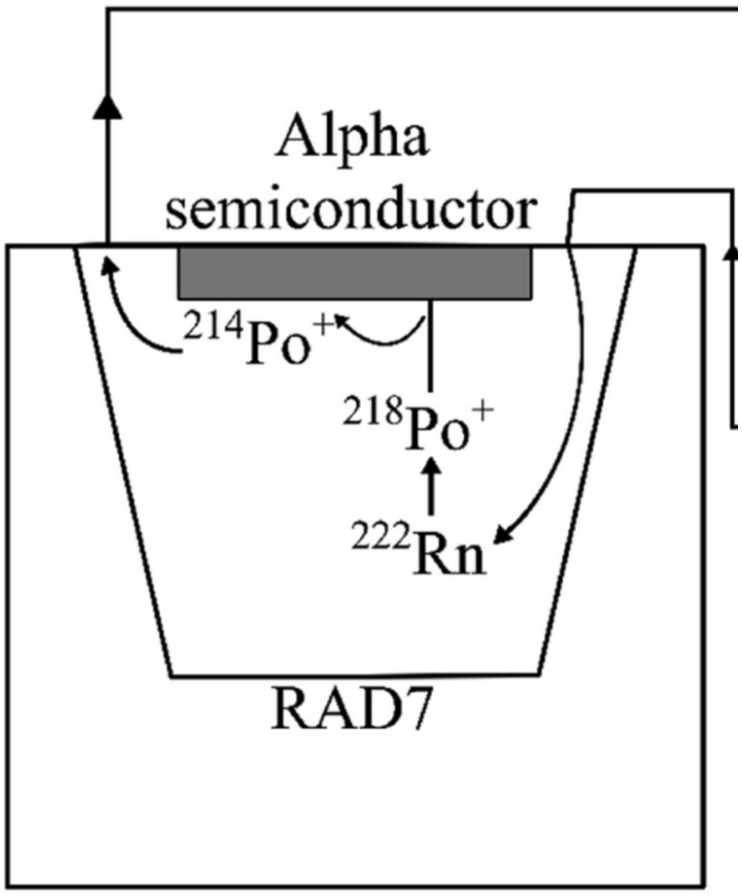

Figure 2.3: Schematic of the RAD7 chamber. Positively charged radon progeny such as ^{218}Po are attracted onto the detector.

When the radon and thoron daughters, deposited on the surface of the detector, decay, they emit alpha particles of characteristic energy directly into the solid-state detector. Since the direction of the emitted alpha particles is random, the detection efficiency of the detector is less than 50%. The RAD7's microprocessor picks up the signal and stores it according to the energy of the particle. The accumulation of many signals results in a spectrum.

More details of the RAD7 are in the manual and references [19] [20]. The RAD7 calculates thoron con-

centration on the basis of the count rate in the spectrum window which is centered on the 6.78 MeV alpha line of ^{216}Po, the first decay product of thoron gas. [21]

2.1.1 Radon progeny collection chamber

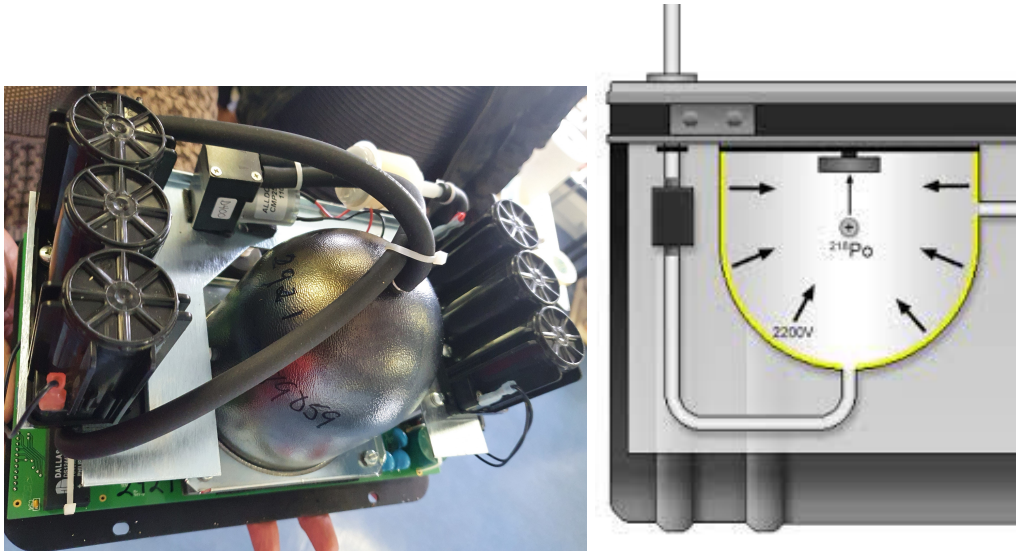

Figure 2.4: (a) Collection chamber (dome-shaped detector system). Figure 2.4. (b) shows the detector chamber.

Before using the RAD7, the first step is purging which means to remove undesired moisture and old radon from the measurement chamber. This can be done by connecting a desiccant to the RAD7 instrument with tubes. The Drierite Gas Purifier is an all-purpose drying unit for the efficient and rapid drying of air. It is used to maintain a dry atmosphere in storage spaces, vaults and commercial packages. Drierite is impregnated with cobalt chloride. It is blue when dry and changes to pink upon absorption of moisture [22].

The need of purging is only to obtain relative humidity less than 10%, so that we can collect accurate results. Moisture in the air reduces the collection of the radon daughters dramatically since it neutralises them. Purging can be simply done by connecting the inlet of the RAD7 at bottom of desiccant drying unit and outlet of the RAD7 at the top of desiccant drying unit. If relative humidity becomes less than 10% it implies that the RAD7 is now ready for use. The RAD7 detector was configured to sniff protocol and grab mode, which permits detecting rapid changes in radon concentration by concentrating on the Polonium concentration and not the radionuclides further down in the decay chain.

The gas particles are sucked or drawn up through the tube into the internal accumulation chamber of

the measuring instrument for 5 min pumping phase during which electrostatic collection of alpha emitters with spectral analysis take place. Alpha emissions with energy of 6.00 MeV attributed to ^{218}Po decay allowed ^{222}Rn activity to be calculated.

2.1.2 Performance and Calibration of RAD7 by Durridge

The RAD7 has to be calibrated by Durridge every 12 to 18 months. After a calibration run, the test RAD7 can be assigned a calibration coefficient that can be applied to future measurements made by that instrument. The calibration coefficient is the mean ratio of the subject RAD7 concentration reading divided by the average reading of two standard RAD7s.

The alpha spectrum should show two clear peaks, at 6.00 and 7.68 MeV, for ^{218}Po and ^{214}Po, respec-

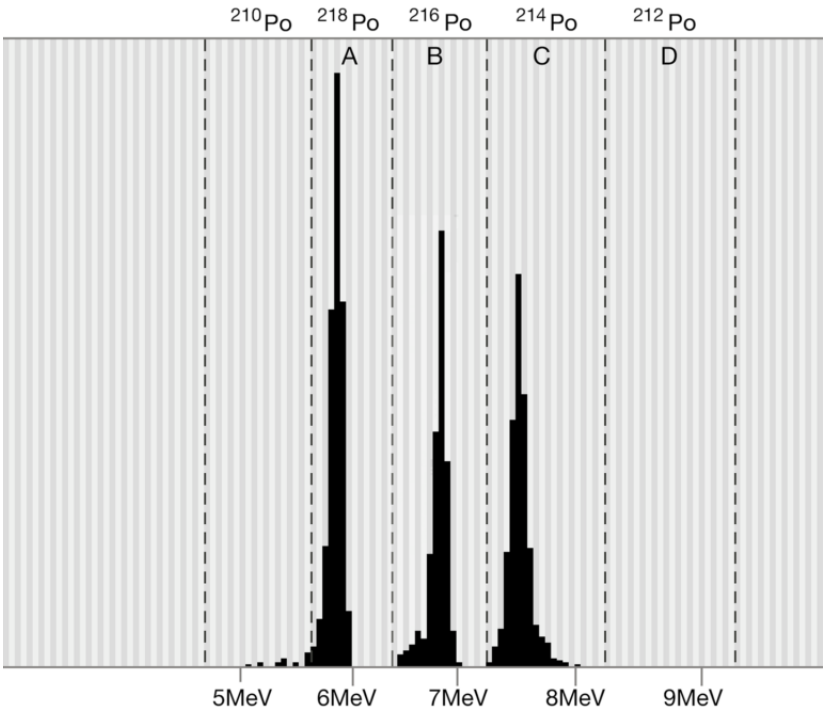

Figure 2.5: Alpha energy spectrum [23].

tively. The actual spectrum in window A is normally a single well-structured peak centered at 6.00 MeV. Peak tails, which may be caused by contamination on the detector surface or electronic noise.

The Quality Control (QC) parameters, such as the high voltage level (2200–2300 V), temperature (20–30

C depending on the room temperature), and leakage current (10–30 nA) should remain fairly steady within their typical ranges. We also require that the concentrations measured by the two standard RAD7s should agree within 2 %. If any of the above criteria are not satisfied, it indicates a problem with either the system or the RAD7s, which may invalidate the calibration. The uncertainty of the efficiency determined by Durridge is reported to be ± 2 % [23].

2.1.3 Radon detection system used at SNOLAB

Some of the most sensitive detectors used to measure radon emanation are situated at SNOLAB where they are used to measure extremely low radon emanation [24] for the nEXO project. These detectors work on exactly the same principle as the RAD7. Air is pumped into a chamber and the radon daughters are attracted to a Si detector. The much higher sensitivity than the RAD7 is achieved by having a much larger volume (4L) and running at reduced pressure to allow the daughters to be attracted to the negatively charged detector [24].

2.1.4 Other equipment used and how its parameters affect radon emanation

The strength of radium escaping through the pores of the rubber or rock sample depends not only upon the total concentration of radium atoms present per unit mass but also upon the fraction of those atoms in the rubber and rock which are located in the matrix or on the rock surfaces so that the newly formed radon atoms can escape into the pores and capillaries [25].

A number, [26] [27] [28] of papers discuss the emanation coefficient in the context of radon in soil leading to radon in houses. Furthermore, there is a published report that states that the emanation rate of radon is influenced by the condition of soil and its porosity, moisture content, temperature and atmospheric pressure [26]. If the moisture content is very low, then the radon release is decreased by the effect of re-adsorption of the radon atoms on surfaces in the pores [27]. Diffusion is identified as the principal method by which radon is transferred into and out of the atmosphere and appears to be relatively independent of insulating materials and vapour retarder. The dispersion of radon in air is influenced by the vertical temperature gradient, the direction and strength of the wind and the air differences [29].

In other work it was found that the variability of radon and correlations with differential pressure gradients may be related to air current in block walls and soil that interrupted radon diffusion inward [28]. It was also found that the effect of turbulence reduces the radon concentration when using a mixing fan [30].

2.2 Pressure measurements needed to be taken in some of our experiments.

The manometer, one of the earliest pressure measuring instruments, when used properly it could potentially produce accurate results. Pressure measurement is the measurement of an applied force by a fluid on a surface. This measuring equipment was implemented to accurately measure pressure for the purpose of this project. Manometers operate on the Hydrostatic Balance Principle: a liquid column of known height will exert a known pressure when the weight per unit volume of the liquid is known. The fundamental relationship for pressure expressed for change in pressure of a liquid column manometer:

$$\Delta P = \rho g \Delta h \tag{2.1}$$

where, P is the pressure on the liquid at height $h; \rho$ is the liquid's density and g is the acceleration due to gravity. Pressure determinations are made by how the fluid moves when pressures are applied to each surface.An inverted manometer is used to measure pressure differences in liquids. Air or another gas fills the space above the liquid in the device and can be bled or expelled through the top to adjust its level. The equation is:

$$P_{\mathrm{L}} - P_{\mathrm{R}} = (\rho_{\mathrm{L}} - \rho_{\mathrm{L}})gh \tag{2.2}$$

where P_{L} is the pressure on the liquid in left leg; P_{R} is the pressure on the liquid in right leg; ρ_{L} is the density of liquid in the left leg and ρ_{R} is the density of liquid in the right leg.

The principles of manometry are demonstrated in the U tube manometer shown in Figure 2.5. It is a glass tube bent to form the letter U and partially filled with some liquid. With both legs of the instrument open to atmosphere or subjected to the same pressure, the liquid mercury maintance exactly the same level or a zero reference.

As illustrated in Figure 2.5, if a pressure is applied to the left side of the instrument, the fluid recedes in the left leg and raises in the right leg. The fluid moves until the unit weight of the fluid as indicated by h exactly balances the pressure. This is known as hydrostatic balance. The height of fluid from one surface to the other is the actual height of fluid opposing the pressure.

The pressure is always the height of fluid from one surface to the other regardless of the shape or size of the tubes. Because of the variations in volume of the manometer legs, the distances moved by the fluid

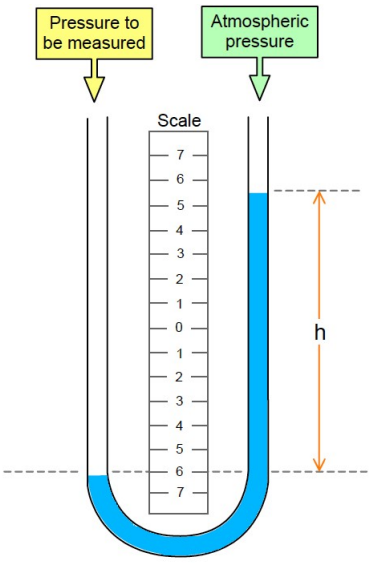

Figure 2.6: U-tube manometer

columns could be different. When pressure is applied to one leg, the liquid is forced down in that leg and up in the other. The resulting pressure is the difference between forces exerted per unit of surface area of the liquid columns, with newtons per square meter (pascals) as the unit. This is independent of variations in tube thickness and shape.

Chapter 3

Experiments using heavy mineral rocks and butyl rubber

3.1 Radon build up in a closed container.

As part of our study into Rn emanation, several experiments were performed in order to build up expertise in radon measurements.

Since radon is produced continuously from the decay of radium in natural decay chain of uranium, the rate of change of the number of radon atoms is determined by radon decay and the generation of radon in the decay of radium present in a closed system such as presented in Fig 2.2. Since radium is present as solid and radon as gas, in order to find the rate of change of the number of radon atoms in the air-filled pore space, we assume that [31] [32]:

·The radium is only present in the sample and decays.
·The radon production and decay in the air space.
·Radon-tight containers, no leakage of radon out of the system and no back diffusion effects.

The decay of radium can be described by the rate equations for radioactive decay:

$$\frac{dN_{\mathrm{Ra}}}{dt} = -\lambda_{\mathrm{Ra}} N_{\mathrm{Ra}} \tag{3.1}$$

If we equate this to the radon production, the rate equation for radon becomes:

$$\frac{dN_{\mathrm{Rn}}}{dt} = \lambda_{\mathrm{Ra}} N_{\mathrm{Ra}} - \lambda_{\mathrm{Rn}} N_{\mathrm{Rn}} \tag{3.2}$$

where λ_{Ra} , λ_{Rn} is the decay constant for radium and radon respectively. $\mathrm{T}_{\mathrm{Ra}\ \frac{1}{2}}$=1600 years, $\mathrm{T}_{\mathrm{Rn}\ \frac{1}{2}}$= 3.824 days are the half-lives for radium and radon respectively.

From Eqs. (3.1) and (3.2), we can determine the number of radon atoms at a time t. By solving two equations, we will obtain the remaining number of radon atoms at any time:

$$N_{\mathrm{Rn}}(t) = \frac{\lambda_{\mathrm{Ra}}}{\lambda_{\mathrm{Rn}} - \lambda_{\mathrm{Ra}}} N_{\mathrm{Ra}}(0)(e^{-\lambda_{\mathrm{Ra}} t} - e^{-\lambda_{\mathrm{Rn}} t}) \tag{3.3}$$

$\mathrm{N}_{\mathrm{Ra}}(0)$, is the original number of radium atoms. The activity A(t) at time t is defined mathematically:

$$A(t) = \lambda N(t) \tag{3.4}$$

Eq. (3.3) becomes:

$$A_{\mathrm{Rn}}(t) = \frac{\lambda_{\mathrm{Rn}}}{\lambda_{\mathrm{Rn}} - \lambda_{\mathrm{Ra}}} A_{\mathrm{Rn}}(0)(e^{-\lambda_{\mathrm{Ra}} t} - e^{-\lambda_{\mathrm{Rn}} t}) \tag{3.5}$$

$\mathrm{A}_{\mathrm{Ra}}(0)$ is original activity of radium which is a constant value.
Since $\mathrm{T}_{\mathrm{Ra}\ \frac{1}{2}} \gg T_{\mathrm{Rn}\,\frac{1}{2}} \longrightarrow \lambda_{\ \mathrm{Ra}} \ll \lambda_{\ \mathrm{Rn}}$ and $\mathrm{e}^{-\lambda t} \longrightarrow 1$ for small t.
Therefore, Eq. (3.5) becomes:

$$A_{\mathrm{Rn}}(t) = A_{\mathrm{Ra}}(0)(1 - e^{-\lambda_{\mathrm{Rn}} t}) \tag{3.6}$$

From Eq. (3.6) the activity of radon grows and becomes exactly the same as the original activity of radium when time t passes many radon half-lives (i.e. $\approx$ 27days). In other words, after this time radon atoms are decaying at the same rate at which they are formed. This is called secular equilibrium [33]. The secular equilibrium is important for the calculation of the activity concentration of radon in the can technique. This means that, the radon activity will reach maximum value or steady state value or equilibrium state value after about 4 weeks. This value is called the final activity or the saturated activity. In other words, we can replace $\mathrm{A}_{\mathrm{Ra}}(0)$ by the steady state (final) activity of radon A_{s} in Eq. (3.6) to become:

$$A_{\mathrm{Rn}}(t) = A_{\mathrm{s}}(1 - e^{-\lambda_{\mathrm{Rn}} t}) \tag{3.7}$$

Eq. (3.7) describes the buildup of radon activity through time t. If V is the volume of air-filled space within the measurement system, the activity concentration of radon C ($\mathrm{Bq{\cdot}m^{-3}}$) in the air volume is given by the

following relation:

$$C = \frac{A_{\mathrm{Rn}}}{V} = \frac{\lambda_{\mathrm{Rn}} N_{\mathrm{Rn}}}{V} \tag{3.8}$$

Eq. (3.7) then becomes:

$$C_{\mathrm{Rn}}(t) = C_{\mathrm{s}}(1 - e^{-\lambda_{\mathrm{Rn}} t}) \tag{3.9}$$

Where C(t) is the radon concentration at time t ($\mathrm{Bq{\cdot}m^{-3}}$) , $\mathrm{C_s}$ is the steady state (final) concentration ($\mathrm{Bq{\cdot}m^{-3}}$) . Eq. (3.9) is the well-known equation which describes the buildup of the concentration of radon emanated from each sample inside the exhalation container with time. Note that $\mathrm{C_s}$ is related to the number of radon atoms emanating from the sample divided by the volume of the measuring system.

One set of experiments used rocks from a mine situated 330 km away from Cape Town to measure thoron [34], the radon isotope with a mass number of 220 and a half-life of 55.6 s, as a preparation towards understanding how radon [35] escapes the rock and what influences the ^{222}Rn, which has a half-life of 3.8 days. The mine contains one of the largest monazite deposits in the world. The data that will be obtained from this experiment will set the tone for the actual rubber experiment for comparison. The short half-life of thoron is an advantage since equilibrium is obtained much sooner.

3.2 Radon emanation measurements of the rock sample and rubber sample

Figure 3.1: The rock sample and butyl rubber sample.

The rock sample experiment was conducted using a stainless steel chamber (where the rock was placed in) that was linked to a RAD7 and the Drierite desiccant in a closed loop as shown in Figs 2.1 and 2.2. The butyl rubber sample was also placed in the chamber where it would exhale radon that would go to the detector through the RAD7's pump.

This is the only counting system used for both radon and thoron in this study. The detector in the RAD7 differentiates between radon and thoron by measuring the alpha energies from ^{218}Po and ^{216}Po, respectively as explained in Chapter 2. The monitor was questioned for the accuracy of its thoron measurements as there were suspension of leakage but it gave reasonable values once the pump was working properly.

The thoron was measured according to the standard operating instructions using a small drying tube. The thoron concentration in some rocks from the mine was also estimated by measuring gamma rays from the ^{232}Th progeny. Thoron exhalation was measured by allowing the thoron to build up in the chamber which was linked to the RAD7 detector as shown in Fig 2.1. Prior to starting the experiment, the system was flushed with nitrogen to remove any radon in the chamber.

3.3 Low Sensitivity Measurements of the butyl rubber from nEXO

The butyl rubber experiment was conducted, similar to the rock experiment, using the chamber that was linked to a RAD7 and the drying unit gas purifier in a closed loop. The butyl rubber was placed in the chamber where it would be sniffed by the RAD7's pump. Radon exhalation was found by allowing for the radon to build up in a chamber which was linked to the RAD7 detector. Prior to starting the experiment, the system was flushed with nitrogen.

A summary of the values that were measured for both experiments at different pressures and different environments will be presented and discussed in the next chapter. The measurements were performed using a manometer to set the pressure [36] at 80 kPa, 90 kPa and 100 kPa for an experiment with the rock. The rock was found at one section in a passage in the mine where the monazite vein is found. The experiments were conducted to find out mainly two things, firstly whether lowering the pressure would increase the radon escape from the rock and the butyl rubber sample [37] (that was was sent from Canada) and secondly to investigate how the data change in an argon environment to see if the atmosphere affect the emanation.

In addition, the rock and the butyl rubber were exposed to argon for comparison to the normal air measurements. Many tests have validated the air-tightness of the chamber and the possibility of adjusting a stable radon activity concentration to a required level over several days [38]. However, these experiments were done at high radon activities where small leaks would not have been noticed.

Chapter 4

Results and Discussion

4.1 Introduction

This chapter presents the results and the analysis for this study. The results were obtained using the RAD7 to measure radon emanation, mainly using the set-up described in Chapter 2 and shown in Fig 2.1 and Figure 2.2. The measurements were done on two samples with different properties and make. The first set was to see if the RAD7 system was able to measure the radon emanation accurately from a rubber sample that was supplied to us by the collaborators from the nEXO project. This rubber has been used as a standard to compare different measurement setups. The rubber has low activity (4 Bq/m^3 per day) and as will be discussed below, the emanation turned out to be too low for our standard setup. Lower limit of detection (LLD) means the smallest amount of sample activity which will yield a net count for which there is confidence at a predetermined level that activity is present.

In a second series of experiments, the emanation from a very active rock, from a monosite seam that is high in thorium was studied. The thoron emanation from this rock is high so that small leaks can probably be ignored and the thoron from the background is so low that it can be ignored. The main aim of these experiments were to test the influence of other variables on the emanation, such as pressure differences and the atmosphere used.

Most experiments that measure radon emanation from materials used in nEXO are done at specific temperature, pressure and atmosphere [37]. This does not correspond to the real situation of these materials in liquid Xe. The experiments in this thesis considers some of the effects on emanation of different atmosphere

and pressure.

The emanation coefficient depends on the radon concentration, temperature, pressure and the porosity of the material [39]. Radon levels in air vary both over time and geographically [17]. Research has found that increasing temperature causes an increase in radon exhalation to the atmosphere [39]. This thesis is investigating what happens in a controlled environment in a case of decreasing the pressure. A hypothesis is that when the pressure inside the chamber is reduced, it creates an environment in which air is drawn more forcefully between the high and low pressure areas and this can pull more air from the rubber or the rock which will increase radon emanation.

From this, an observation can be that air is either sucked (radon is forced out) from the rock and rubber or pushed (radon is pressed) into the rock and the rubber [40]. There are two possibilities, one is that the radon air is pulled out or pushed in the material, as radon can escape from solid materials. There is a principle that supports this known as the "suction effect", which states when the air pressure inside the chamber is lower than the pressure within the rock or rubber, more air will be drawn out of the rock or rubber into the chamber (which subsequently increases the radon concentration in the chamber) [40].

4.2 Background Measurement

In any experiment of emanation it is important to check on the background emanation from the system, detector and possibly small leaks.

Through experimental data, we also sought to determine whether argon or nitrogen gas introduced to the system would have any effect on the radon emanation from the sample. An experiment was conducted to measure the background since radon may be emanating from the chamber walls, welding or any other part of the system. In some cases, nitrogen was flushed through the system before any experiment could be conducted. Once the experiment is completed, the background data can then be subtracted from the data collected from the sample measurements.

Fig 4.1 shows the results of the background measurement. The radon concentration increased steadily indicating that the materials used in our set-up do give off radon at a substantial rate. The fit using the model of Eq. 3.9 indicates a C_s value of 35.7 $Bq.m^{-3}$ that corresponds to a radium source of strength 0.5 Bq. This implies that there are about 30 radon atoms released per minute without any material to be measured.

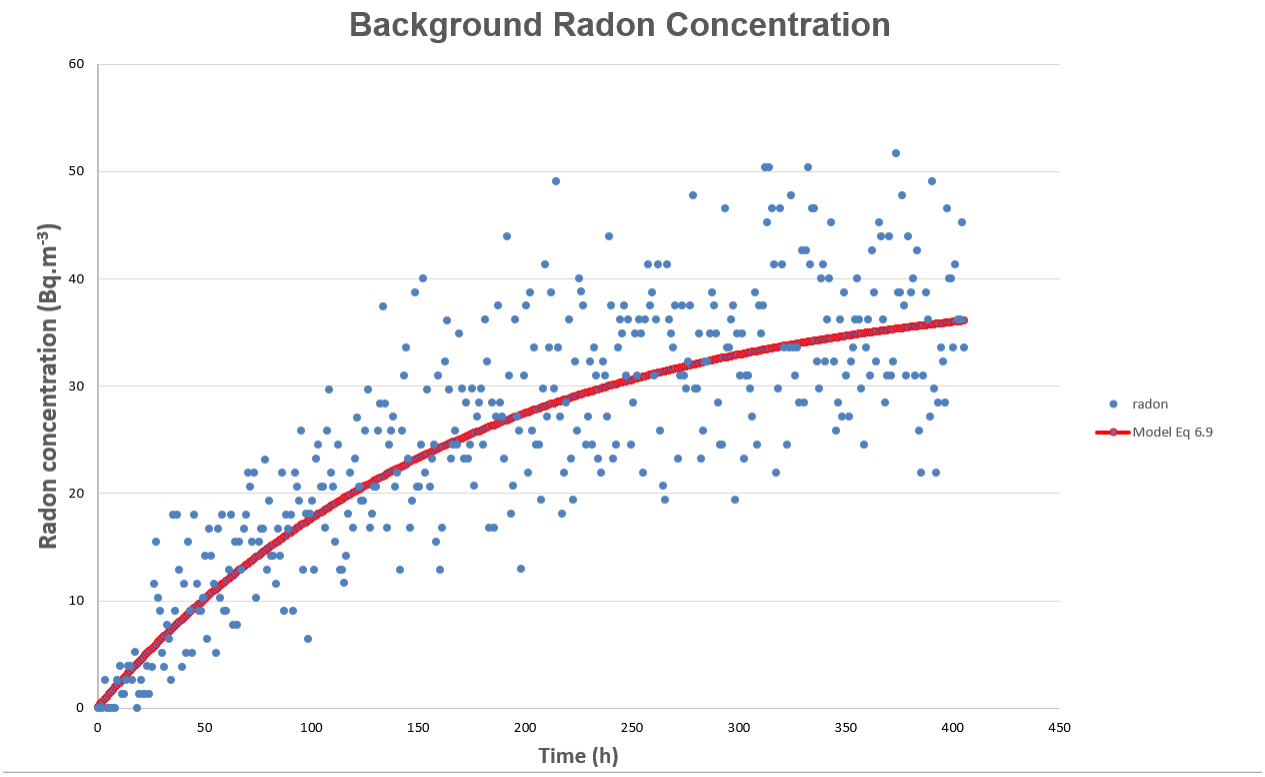

Figure 4.1: The solid line is a model fit according to Eq. 3.9 with C $_s$ = 35.7 $Bq.m^{-3}$. Error bars on the data have been suppressed for clarity. The spread in the values give a good idea of the uncertainties. The uncertainty in C_s is 1.0 as calculated in Appendix A.

4.3 Experiments to measure radon emanation from the rubber

The measurements of the butyl rubber sample will be discussed in this section.

4.3.1 Experiments at Normal pressure and with an air atmosphere.

The results of a measurement of the rubber sample in the chamber at room pressure and with an atmosphere of normal air are shown in Fig 4.2 (red dots). The best fit to this data gives a C_s value of 41.2 Bq.m^{-3}. From the figure where the background is also shown as blue dots, it is clear that the signal is much lower than the background. A statistical analysis similar to the one in Appendix A for the background, gives an uncertainty of 1.5 Bq.m^{-3}. From this value and the result of the background measurement it is clear that the high background makes any calculation of the real signal by subtracting the two very close values ($41.2 \pm 1.5 Bq.m^{-3} - 35.7 \pm 1.0 Bq.m^{-3}$), untrustworthy due to this background. The uncertainties that were taken into account above are purely statistical and any systematic problem from one measurement to the next would invalidate the result.

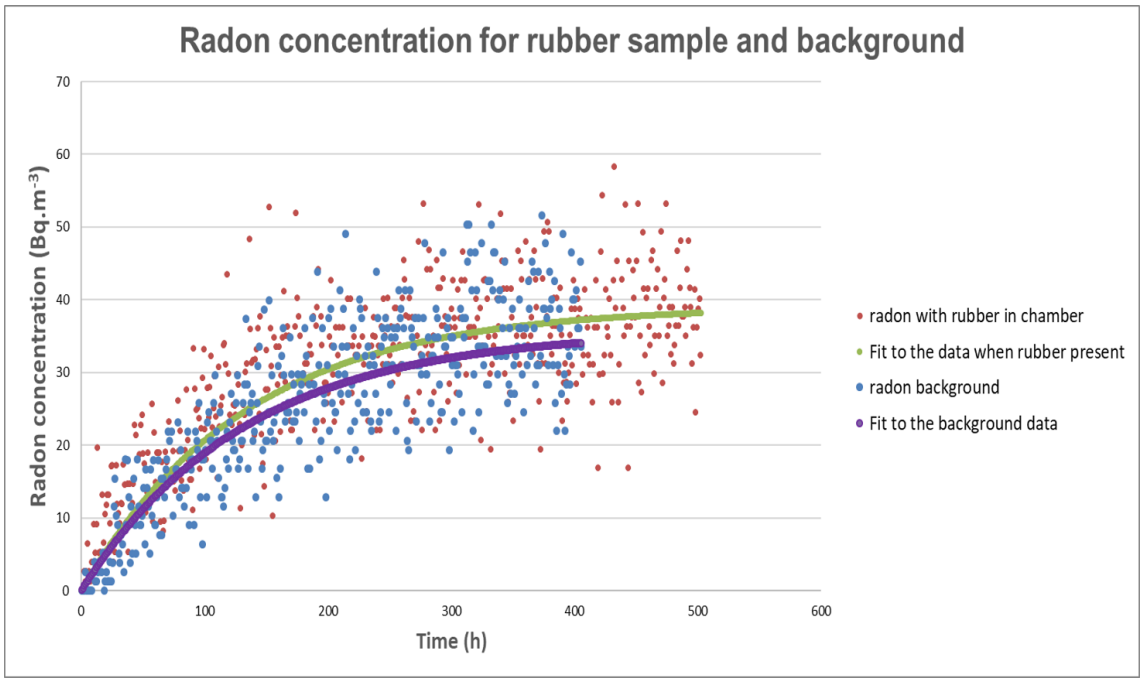

Figure 4.2: Comparison data of the background and radon concentration in the system for the rubber sample at standard temperature and pressure in air atmosphere compared to the background measurement.

4.3.2 Emanation from rubber in Nitrogen atmosphere.

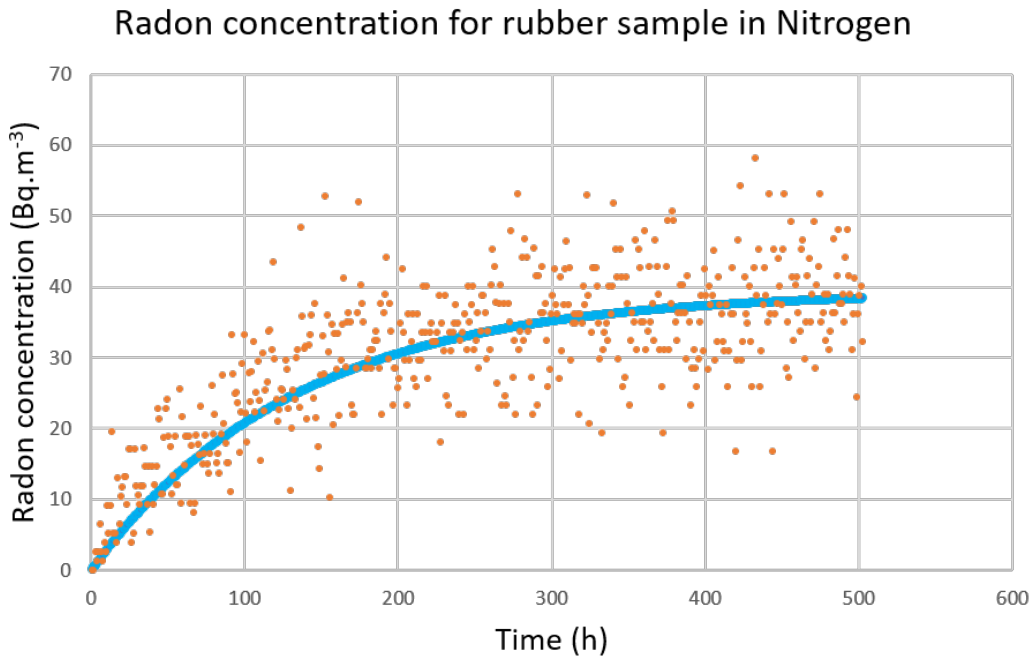

Figure 4.3: Radon growth in the chamber in a Nitrogen atmosphere. The line is a model fit using Eq. 3.9 with C_s =39.3$Bq.m^{-3}$. Error bars have again been suppressed for clarity and the spread of data give an idea of the uncertainties. Note that this measurement was for a shorter period than the ones shown in Fig 4.1 and Fig 4.2.

The result in Fig 4.3 indicates that the radon emanation from rubber seems to be lower in a nitrogen atmosphere, but again the difference is not enough to indicate a definite conclusion. The radon emanation from the rubber is not high enough to give a definitive answer since the emanation from the rubber is only a small contribution to the rise in radon concentration; the main increase due to the increase in the background.

4.4 Experiments to measure thoron emanation from the rock.

In view of the problems with a weak source such as the rubber, we rather used a rock which is a strong emitter of thoron to study emanation. Despite the high activity of thoron, it is always a challenge to measure thoron due to its short half-life. It decays very fast and as a result fails to fill the whole volume of the detection system. Even the chamber of the RAD7 detector does not reach the same concentration as the concentration of the air entering the chamber. This requires a correction factor as discussed in the Appendix

A of the RAD7 manual.

4.4.1 Sample measurements at standard air pressure

When radium decays, the radon that is formed may move into the "pore" space from where it can diffuse out. Emanation is the process in which atoms escapes a material through its concentration gradient from an area of high concentration to an area of low concentration. This is governed by the source strength, which is defined as the number of atoms generated within a material. The ability of atoms to escape a material is dependent on the source power, porosity, temperature and possibly pressure (the amount of particles free versus those closely packed together).

The exhalation rate of ^{222}Rn or ^{220}Rn from a material in an enclosed system is defined by the escape

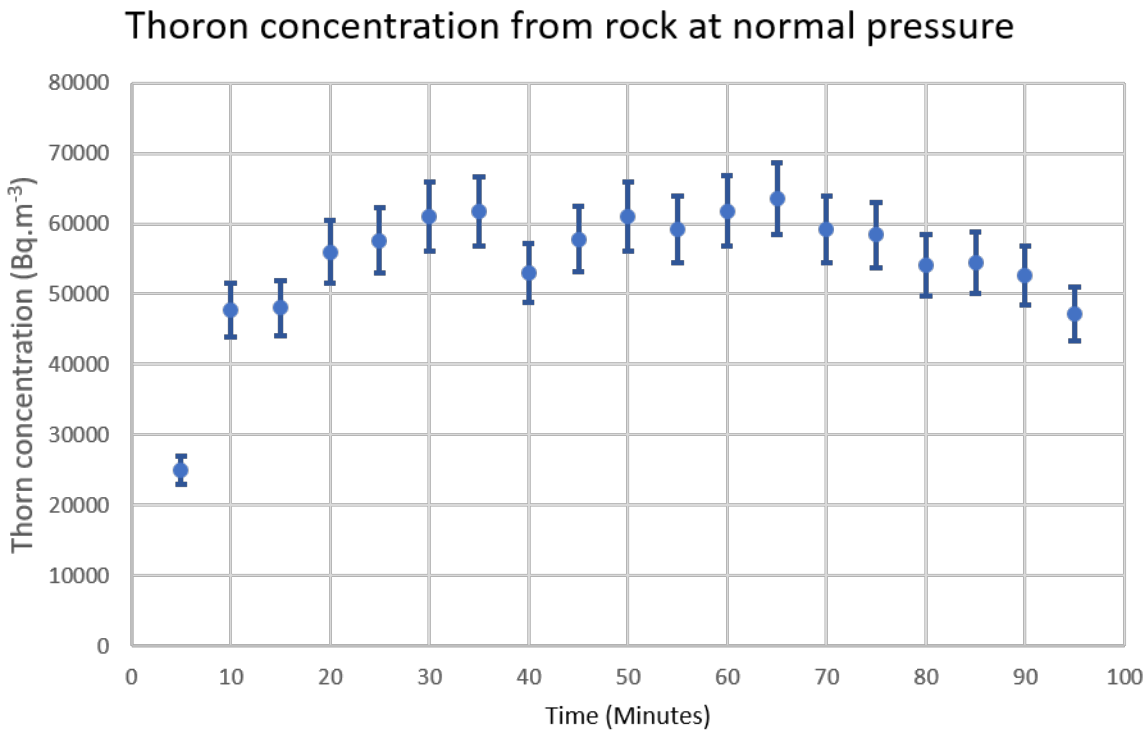

Figure 4.4: The figure provides the thoron concentration as measured with monazite rock in the chamber. Note that the lower value after 5 minutes is probably due to the time taken for the thoron to fill the detector and not due to the half-life of thoron).

of the radon atoms from the surface of the material, per unit area, into the air within the system per unit

time. The atoms that are able to escape the material diffuse from an area of high concentration to an area of low concentration. In a closed system, air is not allowed to enter or exit the system.

The UWC setup was designed in such a way that when measuring a sample, the particles that escape the sample are retained within the system which allows the build up of particle to populate the chamber and spreading out. Fig 4.4 shows the thoron concentration measured with the rock, of mass 1.3 kg, in the set-up. Note that the time is in minutes, but that equilibrium is reached due to the short half-life of thoron. Eq. 3.9 for the case of thoron for which λ is $0.012s^{-1}$ reaches 97 % of the maximum value after only 5 minutes.

4.4.2 Emanation when sample in an argon atmosphere.

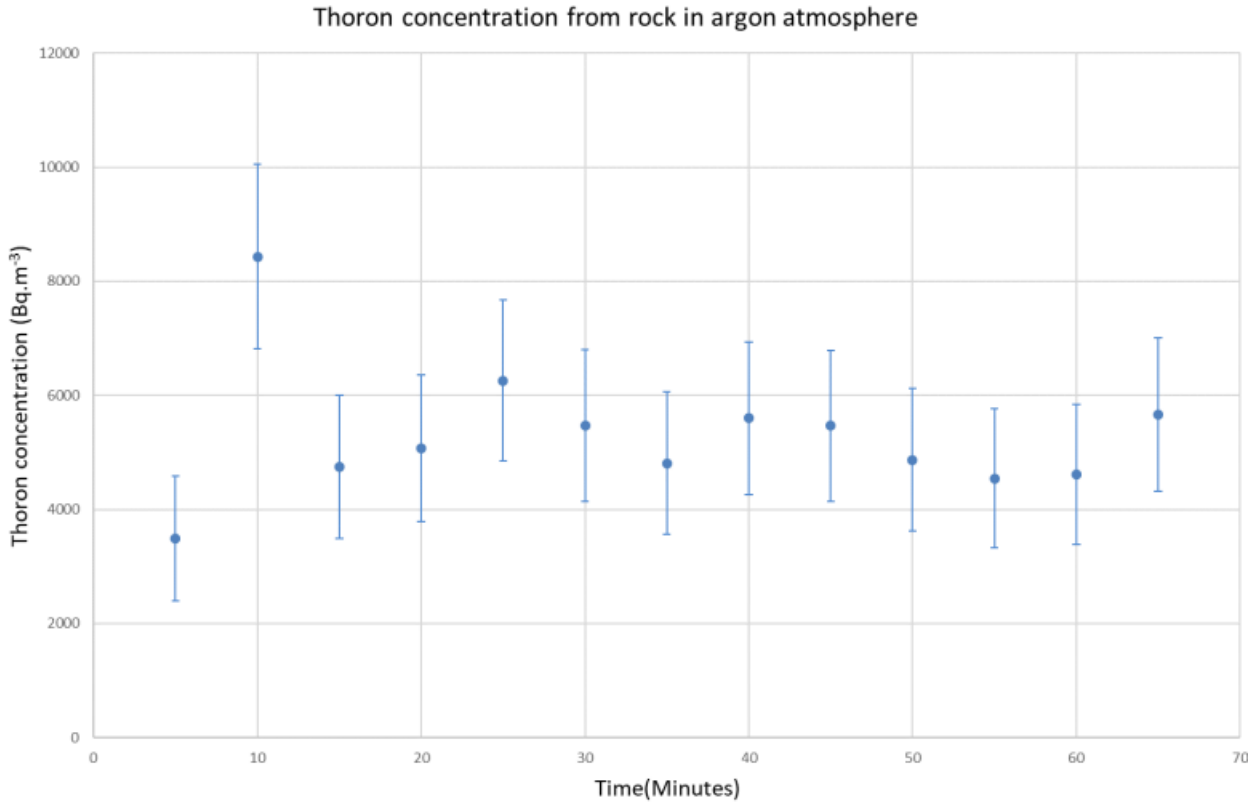

Figure 4.5

Argon was a second choice of gas that was introduced into the system. Argon is found to be about 0.93 % in the atmosphere. Figure 4.5 shows the thoron concentration in the argon atmosphere. This might be due to less resistance in radon gas emanating from the rock and the ability to reach the detector. This is just a preliminary hypothesis that lacks substantial evidence to support it. See Fig 4.5 for the exhalation of thoron

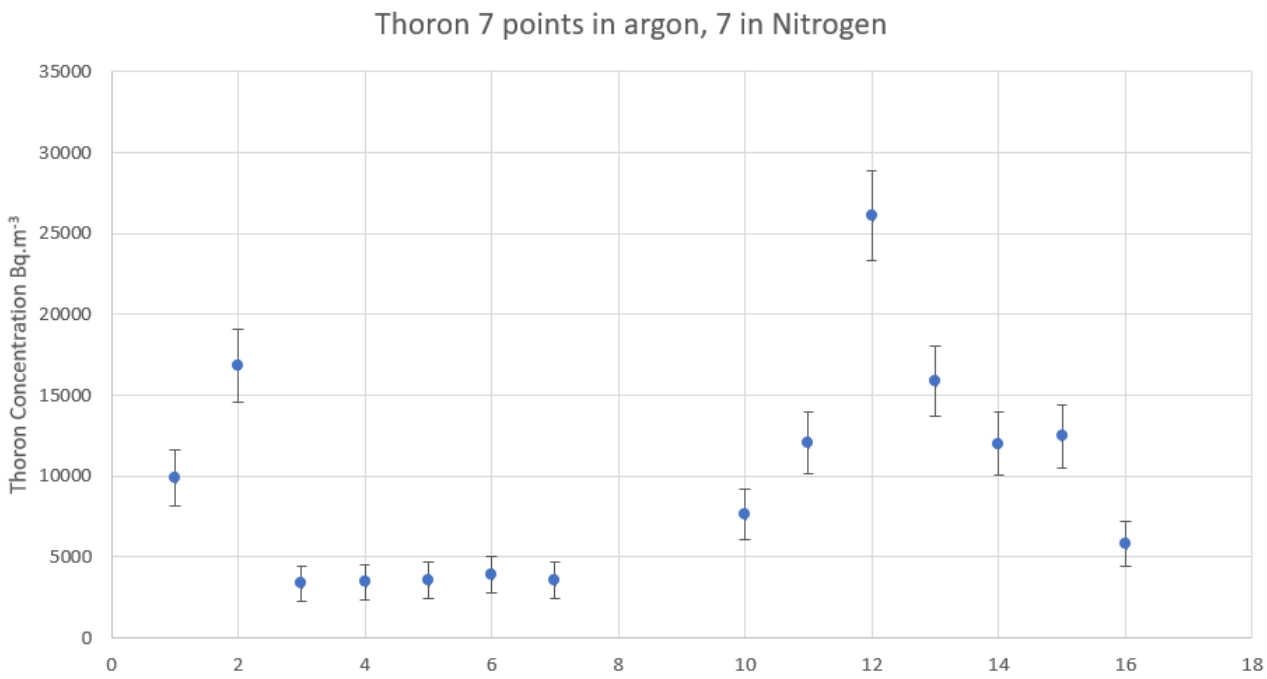

Figure 4.6: Explicitly showing the first 7 data points of thoron in argon atmosphere and last 7 data points of thoron in nitrogen atmosphere.

from the rock in argon atmosphere.

4.4.3 Emanation when the rock sample is in a nitrogen atmosphere.

In order to achieve a clean system, there was a need to remove the existing radon from the detector system. Nitrogen gas was chosen as the method to minimize radon in air and has demonstrated success in past studies [41]. Nitrogen gas from a cylinder was used to flush the detector and chamber to remove any residual radon. Any radon that may have been in the nitrogen cylinder when filled, will have decayed. This means that most air and gas contaminants, including radon, will decrease in concentration when flushed with nitrogen. For this reason, many experiments have used nitrogen gas to purge experimental environments of radon. Nitrogen also has the advantage of reducing the relative humidity by flushing out water vapour.

Figure 4.6 shows the activities of ^{220}Rn as a function of time during the run after flushing the system with nitrogen. Furthermore, Table 4.7. in Appendix B shows the quantitative utility of counts versus time. In Figure 4.6 we observe a decrease in the number of counts of with time after the system was flushed with nitrogen (7 last data points). While pure nitrogen gas has a similar composition to air, which is 78 % nitrogen, and close to zero humidity, the efficiency values using pure nitrogen may be slightly different from

those measured at normal air.

4.5 Study of the influence of pressure variation on emanation.

A fundamental understanding of processes and factors that influence the emanation of ^{222}Rn from a material is essential in the understanding of the operation of the equipment that measures ^{222}Rn emanation. This part of the section will discuss the results of the effect of the lower pressure (or pumping argon gas) into the system on the measurements of the ^{222}Rn emanation. Such experiments may have large uncertainty due to background radiation.

This observation may be accounted by the following: (i) by introducing argon into the system this may affect the chance of radon atoms to escapes and move around the system, (ii) lowering the pressure create an air different between that found within the rock or rubber and the air inside the chamber which may increase the number of atoms that are able to escape (air get sucked out of the rock or rubber) and (iii) the non-homogeneous air particles (that of radon and that of argon [42]) in the system may hinder the emanation of radon atoms as they encounter collisions with other molecules as that gets introduced into the system while the mix.

The first sample test was carried out with a rock sample containing monazite. Although monazite mines are reported to release thoron, all varieties of rocks emit some amount of radon due to naturally-occurring deposits of uranium and thorium in the crust of the Earth. Prior to the first sample measurement, we ran background measurement whereby there was nothing in the chamber to investigate the amount of radiation coming from the walls of the emanation chamber. During the first sample measurement, in which the rock was placed inside the chamber, the valves were closed to allow the build up of radon and circulation of air and gas particle to reach the detector with the assistance of the pump. Fig. 4.7 shows that the initial conditions do make a difference to the first few data points. The short half-life of thoron means that the value rises quickly. There are lower values than in Fig 4.4, which is caused by the position of the sample in the Chamber. As expected the size of the Chamber used in these experiments is too large to give consistent results. The air speed is not fast enough to fill the total space with thoron considering the short half-life of thoron. The different pressures in Fig 4.7 are consistent since the position of the stone in the chamber is the same. But the stone was in a different place compared to the previous experiment leading to very different values for the thoron.

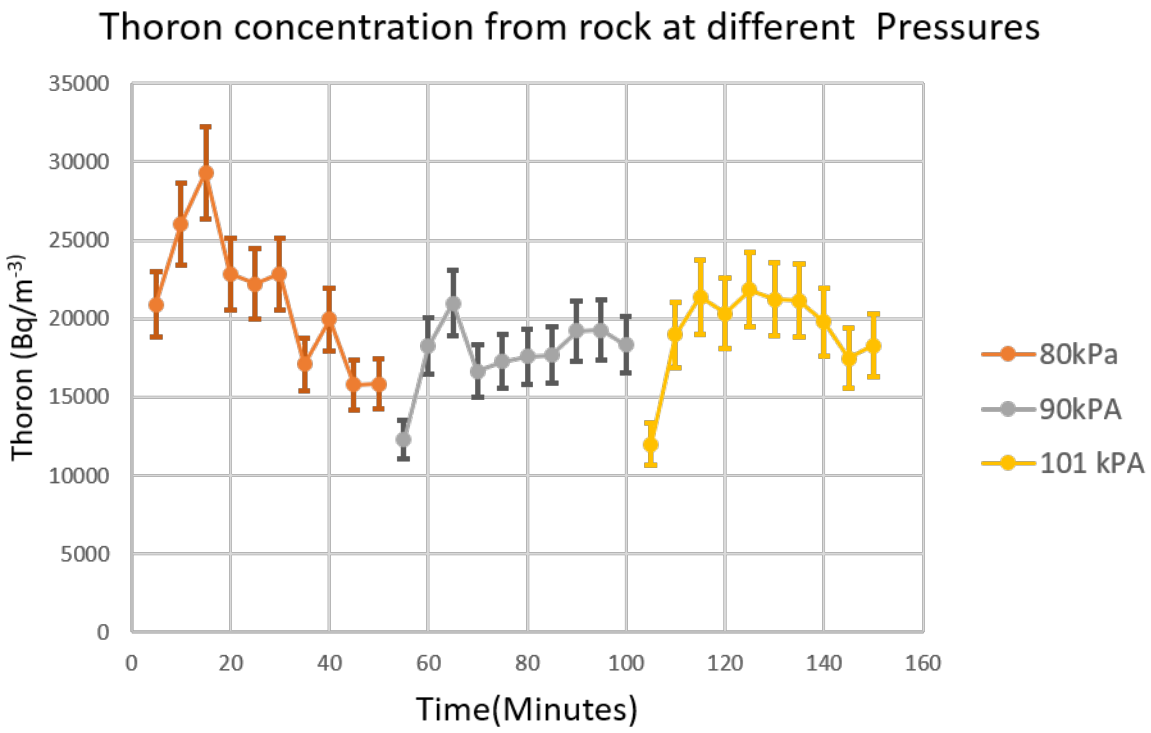

Figure 4.7: Rock sample measurements at different pressure level. The first point in each measurement should probably be ignored since it is linked to the buildup time of the thoron in the detector as discussed below.

4.6 Thoron exhalation from the rock

The exhalation rate of the rubber could not be determined in our experiments due to the large background. The thoron exhalation rate cannot be accurately determined, since the thoron concentration did not fill the entire chamber. However, the data can be used to get a lower limit of the exhalation. Fig. 4.4 show a thoron concentration in the system that stabilized at around 55 000 Bq.m^{-3}. From eq. 3.7 and eq. 3.8, this implies that the value of C_s is at least 55 000 Bq for our system, which with the volume of 14L, implies that the stone acts like a source of 770 atoms of thoron per second. The mass of the stone is 1.3kg and its (irregular) volume is around 400 cm^2. Hence the exhalation (E) from the stone is at least:

$$E = \frac{Act}{Area} \tag{4.1}$$

Where Act is the Activity of the thoron leaving the stone. The decay constant, λ, for thoron is ln(2)/55s Therefore,

$$E = \frac{\lambda \times 700}{400 \times 10^{-4} m^2} = \frac{0.0125 \times 700}{0.04} = 220 Bq.m^{-2}.s^{-1} \tag{4.2}$$

4.7 Discussion.

The experiments aimed at measuring the radon emanation from the rubber were not successful because the background is too high, see from Figure 4.1 - Figure 4.4. To measure meaningful results for the low emanation measurements that are required for the nEXO background measurements, an experimental setup with a much lower limit of detection (LLD) is needed such as achieved in the experimental setup of Jian-Xiong Wang et al. [43].

The experiments that measured the emanation from the monazite rock, measured thoron (^{220}Rn) since the rock has a much larger thorium activity than uranium activity. This has a major advantage since the short half-life of thoron results in equilibrium being reached after only a few minutes as opposed to several days for ^{222}Rn. However, the short half-life has other disadvantages. The volume does not get filled to the same concentration throughout as discussed in some detail in the assessment paperAnan M Al-Karmi et al. [44]. Our measurements of the thoron concentrations show several features which require interpretation.

In Fig 4.6, the thoron has presumably built up to a very high value in close proximity to the stone, but low elsewhere in the stainless steel chamber. When the experiment is started, the concentration is low during the first five minutes while the thoron in the detector is building up. However, when the high concentration of thoron around the stone now reaches the detector, the concentration jumps to a much higher value during the next 5 minutes. The thoron will slowly get distributed more evenly and the initial high thoron concentration around the stone dissipates so that the thoron concentration drops to a more steady state level.

The experiment to consider the pressure changes show that a small change in pressure does not make a major change to the emanation value. There is some indication that a lowering of the pressure leads to an increase in the concentration. There is clearly also a limitation in the use of our large (14L) chamber in the emanation measurements. The short half-life implies that the position of the stone influences the concentration greatly. Hence our different experiments for the rock have very different results except when the conditions were kept the same as in the pressure experiments and the argon followed by nitrogen case.

There is a possibility that as these particles makes their way into the RAD7 chamber, they might encounter the particles found in air which might cause a collision between these particle and slow the positively charged particles down as they bump into other particle, which may result in the loss of their electric charge and

get slowed down before they could reach the detector, consequently losing some counts as observed in the results of the experiment where pressure was increased or a gas was introduced into the chamber. The time radon activity concentration stabilization strongly depends on the volume of the chamber.

Chapter 5

Conclusion

The goal of this research project was to investigate the feasibility of RAD7 detection system to measure (ultra) low levels of radon emanation in materials that that are used in construction of experimental detectors for rare physics search experiments such as NEXT and nEXO. Due to the very reason that radiation, radon, is found everywhere and in all materials it is impossible to completely remove but it can be lowered. Radon is the only daughter in the uranium and thorium decay chains that is gaseous. It is able to escape rock, soil, and materials used in the nEXO time projection chamber by flowing, or diffusing through its cracks and pores.

Radon leads to a source of alpha and beta particles that decay near sensitive detectors, producing a signature (around 2.4 MeV from ^{214}Bi decay) similar to the energy released in neutrinoless double beta decay from ^{136}Xe. This project used a Durridge RAD7 radon detector with a 14L stainless steel chamber to collect radon gas. The detector uses high electrostatic field to collect charged radon decay products on a silicon (Si) photodiode. Radon daughters were collected onto the photodiode, subsequently alpha decays to produce an alpha particle that may be detected. ^{218}Po is the primary ^{222}Rn daughter collected and ^{216}Po is the primary ^{220}Rn daughter collected.

It is important to understand the Rn background activity of the detector and collection chamber itself. A lower background allows a better sensitivity measurement of Rn emanation. Background measurement was performed by observing the activity of radiation coming from the walls of the chamber and detector, the dessicant, pipes and all materials in contact with the air inside the closed loop. A set of measurements were performed with two samples, one with a rock and another with butyl rubber, placed inside the emanation chamber. These experiments were repeated and in addition the systems were individually flushed with

nitrogen and argon. Furthermore, other measurements were conducted with the samples inside the chamber at different pressures.

Based on the results collected from the radon emanation experiments of the samples (rock and rubber), the data demonstrated a possible decrease of the radon emanation when the system was flushed with Nitrogen gas and when the pressure was decreased. Conversely, the results demonstrated an increase of the radon emanation when the system was pumped in with Argon gas and when the pressure was increased, not as high as when the experiment was conducted at standard pressure. The rubber experiment did not work due to high background values. As for the rock experiment, the measurement was successful since there were high values of thoron (but different values depending on the stone position so it is hard to make definite conclusions). To some degree, a hypothesis would be made that introducing different gases and changing the pressure do affect the outcome of the results. These statements are in agreement with other investigations J Farine, et al. [45], but require further investigation.

5.1 Future Work and Recommendations

Future work on this project will include continued emanation measurements of the different sample materials relevant to the construction of the nEXO experiment. This would be done to characterize the different material with their respective emanation signature but will require improved detection limits.

In addition, the work will include integrated detection system consisting of an in-house built liquid xenon vessel and a slight vacuum in a close loop system. The system will allow re-circulation of gases in a controllable way to minimize the loss of circulating gases and refillable gas cylinders, an installed pressure gauge to constantly monitor the pressure change, a thermometer that will monitor the temperature change and an improved sensitive radon detector.

All of these modifications may result in an increased efficiency due to increased likelihood of collecting charged radon (Rn) daughters on the photodiode surface. The effect of temperature and pressure may reduce or increase collection efficiency of the detector. Renewed efficiency measurements in this case will result in better accuracy of Rn emanation measurements.

The matter of low background activity in a system that is searching for a rare events of nuclear processes such as neutrinoless double beta decay ($0\nu\beta\beta$) experiment is not fully understood and requires further investigation. Besides the stainless steel chamber, the purifiers used for EXO construction and the welds or joints in the vessel, the potential sources that contributes to the background events in these experiments are

not fully known and it also requires further investigations.

Bibliography

[1] Mary K Gaillard, Paul D Grannis, and Frank J Sciulli. The standard model of particle physics. *Reviews of Modern Physics*, 71(2):S96, 1999.

[2] John Bernhard Stallo. *The concepts and theories of modern physics*. Harvard University Press, 2013.

[3] Cliff Burgess and Guy Moore. *The standard model: A primer*. Cambridge University Press, 2007.

[4] S Pascoli and ST Petcov. The sno solar neutrino data, neutrinoless double beta-decay and neutrino mass spectrum. *Physics Letters B*, 544(3-4):239–250, 2002.

[5] S Fukuda, Y Fukuda, M Ishitsuka, Y Itow, T Kajita, J Kameda, K Kaneyuki, K Kobayashi, Y Koshio, M Miura, et al. Determination of solar neutrino oscillation parameters using 1496 days of super-kamiokande-i data. *Physics Letters B*, 539(3-4):179–187, 2002.

[6] Kai Zuber. Search for the neutrino mass and low energy neutrino astronomy. In *From Ultra Rays to Astroparticles*, pages 187–213. Springer, 2012.

[7] JD Vergados, H Ejiri, and F Šimkovic. Theory of neutrinoless double-beta decay. *Reports on Progress in Physics*, 75(10):106301, 2012.

[8] Martin Lahrz. The solar neutrino problem. 2009.

[9] Govinda Adhikari, S Al Kharusi, E Angelico, G Anton, IJ Arnquist, I Badhrees, J Bane, V Belov, EP Bernard, T Bhatta, et al. nexo: neutrinoless double beta decay search beyond 1028 year half-life sensitivity. *Journal of Physics G: Nuclear and Particle Physics*, 49(1):015104, 2021.

[10] C Adams, V Álvarez, L Arazi, IJ Arnquist, CD Azevedo, K Bailey, F Ballester, JM Benlloch-Rodríguez, Filipa IGM Borges, N Byrnes, et al. Sensitivity of a tonne-scale next detector for neutrinoless double-beta decay searches. *Journal of High Energy Physics*, 2021(8):1–24, 2021.

[11] S Al Kharusi, A Alamre, JB Albert, M Alfaris, G Anton, IJ Arnquist, I Badhrees, PS Barbeau, D Beck, V Belov, et al. nexo pre-conceptual design report. *arXiv preprint arXiv:1805.11142*, 2018.

[12] WR Armstrong. Cupid pre-cdr. *arXiv. org Repository*, 2019, 2019.

[13] Xavier Carlos Quintana. Radon measurement for neutrinoless double beta decay. 2018.

[14] Eric S Morrison, Therese Frels, Eric H Miller, Richard W Schnee, and Joseph Street. Radon daughter plate-out onto teflon. In *AIP Conference Proceedings*, volume 1921, page 090002. AIP Publishing LLC, 2018.

[15] Maja Lecher. *Exploring the applicability of electrodeposited copper for reducing the radon background in liquid xenon detectors*. PhD thesis, Ruprecht-Karls-Universität Heidelberg, 2019.

[16] Fatih Külahcı and Şerif Çiçek. On the determination of transportation, range and distribution characteristics of uranium-238, thorium-232 and potassium-40: a critical review. *Environmental Earth Sciences*, 78(24):1–29, 2019.

[17] Natasha Dimova, William C Burnett, and Derek Lane-Smith. Improved automated analysis of radon (222rn) and thoron (220rn) in natural waters. *Environmental science & technology*, 43(22):8599–8603, 2009.

[18] Robert R Greenberg, Peter Bode, and Elisabete A De Nadai Fernandes. Neutron activation analysis: a primary method of measurement. *Spectrochimica Acta Part B: Atomic Spectroscopy*, 66(3-4):193–241, 2011.

[19] Yanliang Tan and Detao Xiao. Revision for measuring the radon exhalation rate from the medium surface. *IEEE Transactions on Nuclear Science*, 58(1):209–213, 2010.

[20] G Zuzel and H Simgen. High sensitivity radon emanation measurements. *Applied Radiation and Isotopes*, 67(5):889–893, 2009.

[21] Y Tan, D Xiao, H Yuan, Q Tang, and X Liu. Revision for measuring radon exhalation rate in open loop. *Journal of Instrumentation*, 8(01):T01004, 2013.

[22] Yanliang Tan and Detao Xiao. A novel method to measure the radon exhalation rate in only one measurement cycle. *Analytical Methods*, 5(3):805–808, 2013.

[23] RAD7 RADON DETECTOR DURRIDGE. Owner's manual (bedford, ma.), 2012, 2012.

[24] Joseph Street, R Bunker, EH Miller, RW Schnee, S Snyder, and J So. Radon mitigation for the

supercdms snolab dark matter experiment. In *AIP Conference Proceedings*, volume 1921, page 050002. AIP Publishing LLC, 2018.

[25] Allan B Tanner. Methods of characterization of ground for assessment of indoor radon potential at a site. *Field studies of radon in rocks, soils, and water*, pages 1–18, 1991.

[26] Nabil M Hassan, Masahiro Hosoda, Tetsuo Ishikawa, Atsuyuki SORIMACHI, Sarata K SAHOO, Shinji TOKONAMI, and Masahiro FUKUSHI. Radon migration process and its influence factors; review. *Japanese Journal of Health Physics*, 44(2):218–231, 2009.

[27] Patitapaban Sahu, Devi Prasad Mishra, Durga Charan Panigrahi, Vivekananda Jha, R Lokeswara Patnaik, and Narendra Kumar Sethy. Radon emanation from backfilled mill tailings in underground uranium mine. *Journal of environmental radioactivity*, 130:15–21, 2014.

[28] RS Lively and LF Goldberg. Diffusion of radon through concrete block walls-a significant source or indoor radon. *Radiation protection dosimetry*, 82(1):31–42, 1999.

[29] S Chambers, AG Williams, W Zahorowski, A Griffiths, and J Crawford. Separating remote fetch and local mixing influences on vertical radon measurements in the lower atmosphere. *Tellus B: Chemical and Physical Meteorology*, 63(5):843–859, 2011.

[30] Robert F Holub, Robert F Droullard, Wu-Lieh Ho, Philip K Hopke, Ronn Parsley, and James J Stukel. The reduction of airborne radon daughter concentration by plateout on an air mixing fan. *Health Physics*, 36(4):497–504, 1979.

[31] AF Nader. Theoretical and experimental study to evaluate radioactivity applied on a selected area in basra governorate [thesis]. *Basra, Iraq: University of Basra, Iraq*, 2015.

[32] Haijing Jiang, GE Liangquan, Yanchang Lin, and GU Yi. Preliminary study on a regional radon concentration in surface soil prediction method. *Progress in Nuclear Science and technology*, 1:364–367, 2011.

[33] SH Byun. Radioactivity: Radioisotopes and radiation methodology lecture notes. *Canada: University of McMaster*, 2014.

[34] Robert Lindsay, Elmughera Elhag, Robert J de Meijer, Joash N Ongori, and Peane P Maleka. Thoron standard source. *Applied Radiation and Isotopes*, 147:99–104, 2019.

[35] DB Chambers. Thoron and decay products, beyond unscear 2006 annex e. *Radiation protection dosimetry*, 141(4):351–356, 2010.

[36] F Abu-Jarad and RG Sextro. Reduction of radon progeny concentration in ordinary room due to a mixing fan. *International Journal of Radiation Applications and Instrumentation. Part D. Nuclear Tracks and Radiation Measurements*, 15(1-4):629–632, 1988.

[37] Michelle Nassar, Pedro A Vázquez, Nicolas Chauris, Michel Daaboul, Anny Michel, and Christophe Louste. Experimental models of the variation of hfe-7100 and hfe-7000 electric properties with temperature. *IEEE Transactions on Industry Applications*, 56(4):4193–4199, 2020.

[38] Joash N Ongori, Robert Lindsay, and Mashinga J Mvelase. Radon transfer velocity at the water–air interface. *Applied Radiation and Isotopes*, 105:144–149, 2015.

[39] RA Akber, J Pfitzner, and A Johnston. Wind direction correlated measurements of radon and radon progeny in atmosphere: A method for radon source identification. In *Proceedings of the radon and radon progeny measurements in Australia symposium*, 1994.

[40] Samira Jamalian, Mohammad Jafarnejad, Scott D Zawieja, Christopher D Bertram, Anatoliy A Gashev, David C Zawieja, Michael J Davis, and James E Moore. Demonstration and analysis of the suction effect for pumping lymph from tissue beds at subatmospheric pressure. *Scientific reports*, 7(1):1–17, 2017.

[41] X Yu, C Yu, G An, B Yu, T Hu, L Zhou, X Cai, Y Xie, L Sun, J Fang, et al. Nitrogen purification pilot plant of jiangmen underground neutrino observatory. *Journal of Instrumentation*, 16(08):T08002, 2021.

[42] Shinzou Kubota, Masahiko Hishida, Masayo Suzuki, Jian-Zhi Ruan, et al. Dynamical behavior of free electrons in the recombination process in liquid argon, krypton, and xenon. *Physical Review B*, 20(8):3486, 1979.

[43] Jian-Xiong Wang, Tom C Andersen, and John J Simpson. An electrostatic radon detector designed for water radioactivity measurements. *Nuclear Instruments and Methods in Physics Research Section A: Accelerators, Spectrometers, Detectors and Associated Equipment*, 421(3):601–609, 1999.

[44] Anan M Al-Karmi and MA Morsy. Epr of gamma-irradiated polycrystalline alanine-in-glass dosimeter. *Radiation Measurements*, 43(7):1315–1318, 2008.

[45] TC Andersen, I Blevis, J Boger, E Bonvin, M Chen, BT Cleveland, X Dai, F Dalnoki-Veress, G Doucas, J Farine, et al. Measurement of radium concentration in water with mn-coated beads at the sudbury neutrino observatory. *Nuclear Instruments and Methods in Physics Research Section A: Accelerators, Spectrometers, Detectors and Associated Equipment*, 501(2-3):399–417, 2003.

[46] R Lindsay, S Mngonyama, P Molahlehi, XE Ngwadla, and GJ Ramonnye. Pilot study of thoron concentration in an underground thorium mine. *Health Physics*, 123(4):315–321, 2022.

[47] M Balcázar, A López, T Streil, and A Chávez. Radon leakage assessment in a controlled radon laboratory. *Geofísica Internacional*, 41(3):281–284, 2002.

APPENDIX A

Statistical analysis of fit to the radon data using Eq. 3.9..:

A best fit for the model as given by Eq. 3.9. can easily be obtained by calculating the Chi Square value and using the EXCEL function "SOLVER" to minimise the Chi Square value by changing C_s which is the only free parameter.

$$\chi^2 = \Sigma \frac{(y_i - y_t)^2}{(\sigma_i)^2}$$

where

y_i = the measured radon concentration at point i,

σ_i = the uncertainty at point i,

y_t = the calculated value at point i using Eq. 3.9.

For the background measurement, the obtained value for C_s is 35.8 Bq.m $^{-3}$. By using the usual method of finding the uncertainty in this parameter by looking for the values where the Chi Square (x^2 value) increases by 1, (See e.g. section 3.2.2 in Andrae, R. 2010, ArXiv e-prints 1009.2755), the uncertainty is found to be 1.08 from the calculated values as shown on the plot below. Hence our result is 35.8 ± 1.0 Bq.m^{-3} [46].

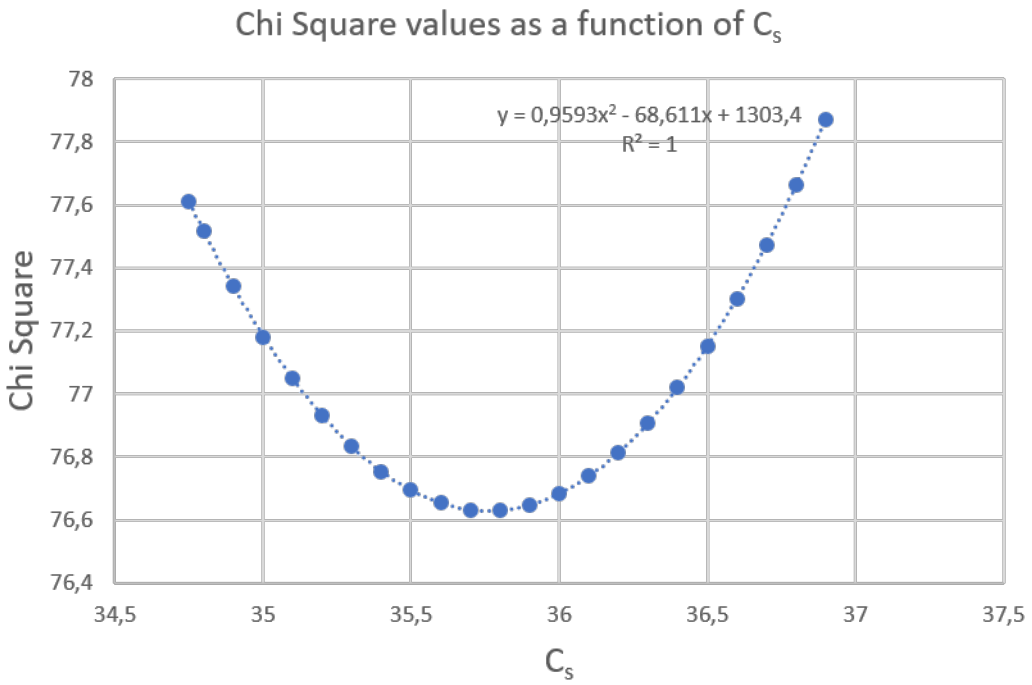

Operation of the RAD7 detector:

This section partly discusses the calibration which Durridge does for us.
The RAD7 radon detector, manufactured by Durridge Co., Inc. (Bedford, MA), is useful for environmental studies because it is portable, durable, very sensitive, and operates in a continuous mode.

The RAD7 has energy window settings that has been chosen to allow one to discriminate all alpha-emitting isotopes including the ^{222}Rn daughters ^{218}Po ($T_{1/2}$ = 3.05 min; E = 6.00 MeV) in window A and ^{214}Po ($T_{1/2}$ = 1.64 s; E = 7.68 MeV) in window C. For faster analyses, the ^{218}Po is preferred as it will reach radioactive equilibrium with ^{222}Rn in only about 15 min. For applications when longer integration times (3 h) are suitable, both ^{218}Po and ^{214}Po can be used to obtain higher precision results. Window B and D are chosen to identify the ^{220}Rn progeny.

The reservoir used in the system is a 12-cm diameter PVC pipe (volume 12 L) closed at both ends and with ports for connections to the rest of the system. This reservoir provides a means to ensure that the radon-enriched gas is well mixed for the RAD7s, both for those under calibration and for the standard instruments dedicated to the calibration system. There are four connectors from the reservoir for access to other parts of the system. Two ports on opposite sides of the reservoir are connected to the inlet and outlet of the radon air flow from the Mn-fiber cartridge.

The third connector is for the RAD7 supply manifold and the fourth port is for the return manifold. When the RAD7 internal pumps are on, air is circulated from the reservoir via the supply manifold, through the RAD7s and returned to the reservoir through the return manifold. The manifolds allow several RAD7s to be connected to the calibration system simultaneously. The inlets of each RAD7 on the system are fitted with an inlet filter, and these are connected to the supply manifold. The RAD7 outlets are connected to the return manifold.

We are using two dedicated RAD7s calibrated precisely at Durridge's in-house system as standards. The benefit of using two detectors as standards is that one can recognize if the efficiency of one of the standards starts to drift. For operation, it is always a good practice to purge the RAD7s before and after a calibration test. First of all, it is helpful to clear the chamber of radon gas and daughters as quickly as possible to prevent their adsorption on internal surfaces of RAD7s.

Using a desiccant-filled drying tube, dry low-radon air is circulated through the chamber in order to re-

move radon from the previous test and to lower the background. University of the Western Cape setup usually start by purging the RAD7s for more than 1 h until the readings in window A are lower than 0.5 cpm(count per minute). Use of the drying tube is necessary during purging and normal operation to maintain low humidity in the RAD7 chamber. High relative humidity leads to detector sensitivity reduction at typical room temperatures. We ordinarily do not start a calibration test until the relative humidity is lower than 10% (typically less than 6%).

After an appropriate holding period in the gas-tight cartridge, radon is degassed from the Mn-fiber ^{226}Ra source by opening all valves in part A and running the external air pump continuously. All RAD7s connected to the system will introduce a certain amount of low-radon fresh air (around 1 L each) to the system. Thus, to make sure all the gas throughout the system is well mixed, all RAD7s connected to the system have their pumps running while the external air pump of Part A is delivering radon into the reservoir.

An adjustable air flow meter placed in the system downstream of the radon source provides a fixed flow rate of 4 L/min. It thus takes about 5 min to replace all the air in the reservoir (12 L) and 8 RAD7s (1 L each so total volume 20 L). However, as the flow is not necessarily first-in-first-out, it may take several volume replacements to ensure that we have a well-mixed radon concentration within the reservoir. To be conservative, we run the external air pump for at least 15 minutes and the close the valves to allow good mixing of the reservoir air with the RAD7s for another 10 minutes. The RAD7s are then reset and the calibration testing is started.

We used a RAD7 counting protocol that included an integration time (cycle time) of 1 h, a recycle number of 20, 'sniff' mode (uses window A, ^{218}Po only) and pump setting of "auto" (air pump runs 1 min out of every 5). Integration times, which can be adjusted anywhere from 2 min to 24 h on a RAD7, should be at least 30 min. Since the RAD7 only measures the 'live time' to one tenth of a minute, using a 2 min cycle and 1.5 min live times would introduce an automatic 6% uncertainty. The 'recycle number' on a RAD7 refers to the number of runs within a test. So with a 1-h integration time and a recycle number of 20 means that the calibration will require 20 h.

The uncertainty of a calibration result will depend to some extent on the length of the test. While longer testing would result in more radioactive decays being recorded and consequently lower counting errors, there are other factors that introduce uncertainties. Based on these observations we chose a 20-h period as an optimum period for calibration. This is also convenient as the system can be started in the afternoon, run overnight, and stopped the following day. The 'sniff' mode is typically used in our research since we desire a rapid response to changes in radon concentration.

In this mode, the RAD7 only uses the 3-min ^{218}Po alpha peak in window A for calculating the radon concentration. In the 'auto' pump setting, the pump always switches on for 5 min at the beginning of a new test cycle to ensure a good initial sample. If the humidity in the sample chamber remains above 10%, the pump stays on until the humidity reaches that threshold. Then the pump runs for 1 min in every five, until the end of the cycle.

Because leaks [47] in the calibration system would likely make the results more variable, leakage tests were performed routinely. Durridge first pressurize the system using a pressure pump and then monitor the pressure to see if it holds under static conditions over a reasonable amount of time. Since the manufacturer recommends that RAD7s should not be run under a positive pressure higher than 5.2 kPa, we perform the leakage tests in two steps, one under higher pressure (80 kPa) without the RAD7s being installed, and then again under lower pressure with the RAD7s in line.

A manometer was used to monitor the pressure. Small drops in pressure, no more than about 0.1 kPa over a 20-min period, were considered acceptable. Higher pressure drops were occasionally encountered and this indicated a leak in the system that was identified and repaired before continuing. Since the system is a closed air loop, only decay and leakage would lead to lower concentrations over time.

APPENDIX B

Table 5.1: Background experiment. Counts in an hour presented every 20 hours for 15 days for the four windows.

Time(h)	Nr of counts in different Windows				Rn Concentration ($Bq.m^{-3}$)
	Window A	Window B	Window C	Window D	
1	0	0	1	0	0
21	1	0	1	0	3
41	5	0	4	1	12
61	2	1	5	0	9
81	8	1	7	1	19
101	10	3	6	2	19
121	9	0	9	0	23
141	10	1	8	2	22
161	5	0	6	1	13
181	9	1	10	0	25
201	12	1	17	1	37
221	13	0	16	3	36
241	14	2	15	0	37
261	17	3	7	1	31
281	13	0	10	1	30
301	11	1	13	1	31
321	19	1	13	1	41
341	11	3	14	0	32
361	14	0	14	1	36
381	18	0	13	2	39

Table 5.2: Rubber sample experiment in normal air at standard pressure

Time (min)	Total number of counts	% of counts in Window A	% of counts in Window B	% of counts in window C	% of counts in Window D	Rn concentration ($Bq.m^{-3}$)
5	59	0	3,4	6,8	0	0
10	66	0	0	12,1	1,5	0
15	58	1,7	1,7	0	0	2,68626
20	66	1,5	1,5	0	0	1,295924
25	51	2	2	3,9	2	2,59645
30	53	5,7	0	3,8	0	6,496895
35	53	3,8	0	0	1,9	2,597603
40	65	1,6	1,6	1,6	3,1	1,300534
45	51	5,9	0	2	2	3,906814
50	52	1,9	1,9	1,9	0	2,603384
55	52	7,7	1,9	5,8	1,9	9,128093
60	62	3,2	0	3,2	1,6	5,216053
65	56	7,2	0	5,4	1,8	9,140316
70	62	14,5	0	9,7	0	19,61266
75	65	3,1	1,6	6,2	6,2	5,227706
80	59	6,8	0	1,7	1,7	5,237066
85	66	3	1,5	1,5	1,5	3,926042
90	57	8,8	3,5	8,8	0	13,11615
95	52	1,9	1,9	7,7	0	6,549265
100	79	5,1	1,3	5,1	1,3	10,51178
105	70	5,7	2,9	7,2	1,4	11,81513
110	69	7,3	1,5	7,3	0	13,17523

Table 5.3: Counts in different windows and thoron concentration in experiment at normal air pressure and in air atmosphere. Note the counts in window "B" corresponding to the alpha particle energy from ^{216}Po.

Time	Counts in Window in 5 min period				Thoron	Thoron Uncertainty
Min	A	B	C	D	Bq.m^{-3}	Bq.m^{-3}
5	14	379	0	0	25000	2700
10	36	716	0	2	47700	3700
15	30	720	0	1	48000	3710
20	41	835	0	4	56000	4010
25	43	854	1	2	57600	4080
30	51	900	0	4	61000	4200
35	49	911	5	2	61700	4230
40	47	787	4	6	53000	3920
45	55	853	3	12	57800	4100
50	47	900	6	4	61000	4200
55	53	874	8	9	59200	4150
60	36	912	7	14	61800	4230
65	46	937	9	12	63500	4290
70	61	873	4	12	59200	4140
75	60	861	11	22	58400	4120
80	52	803	19	19	54100	3960
85	52	810	3	25	54500	3970
90	45	780	10	23	52600	3900
95	60	701	7	29	47200	3710

Table 5.4: Rubber sample in nitrogen gas.

Time (hour)	Total number of counts	% of counts in Window A	% of counts in Window B	% of counts in window C	% of counts in Window D	Rn concentration ($Bq.m^{-3}$)
5	59.	0.0	3.4	6.8	0.0	0.
10	66.	0.0	0.0	12.1	1.5	0.
15	58.	1.7	1.7	0.0	0.0	2.68626
20	66.	1.5	1.5	0.0	0.0	1.295924
25	51.	2.0	2.0	3.9	2.0	2.59645
30	53.	5.7	0.0	3.8	0.0	6.496895
35	53.	3.8	0.0	0.0	1.9	2.597603
40	65.	1.6	1.6	1.6	3.1	1.300534
45	51.	5.9	0.0	2.0	2.0	3.906814
50	52.	1.9	1.9	1.9	0.0	2.603384
55	52.	7.7	1.9	5.8	1.9	9.128093
60	62.	3.2	0.0	3.2	1.6	5.216053
65	56.	7.2	0.0	5.4	1.8	9.140316
70	62.	14.5	0.0	9.7	0.0	19.61266
75	65.	3.1	1.6	6.2	6.2	5.227706
80	59.	6.8	0.0	1.7	1.7	5.237066
85	66.	3.0	1.5	1.5	1.5	3.926042
90	57.	8.8	3.5	8.8	0.0	13.11615
95	52.	1.9	1.9	7.7	0.0	6.549265
100	79.	5.1	1.3	5.1	1.3	10.51178
105	70.	5.7	2.9	7.2	1.4	11.81513
110	69.	7.3	1.5	7.3	0.0	13.17523
115	54.	3.7	3.7	14.8	1.9	13.14562

Table 5.5: Rock sample in argon gas.

Time (min)	Total number of counts	% of counts in Window A	% of counts in Window B	% of counts in window C	% of counts in Window D	Rn concentration ($Bq.m^{-3}$)
5	214	2,8	70,1	0,5	0,5	196,7213
10	326	3,4	78,5	0,3	0,6	329,6508
15	108	8,3	47,2	0,9	1,9	262,295
20	111	11,7	46,9	0,9	3,6	360,6557
25	113	9,7	47,8	3,6	2,7	296,6857
30	122	13,9	48,4	0,8	0,8	560,4063
35	171	14,6	31,6	5,9	3,5	721,3113
40	130	0,8	89,2	3,1	0	32,61062
45	206	2,4	88,8	2,4	2	98,89524
50	439	4,3	88,2	2,5	0,2	636,7178
55	270	3,7	89,3	1,1	1,1	295,082
60	206	2,9	88,4	3,9	1,5	164,8254
65	212	3,8	89,2	2,8	1,9	196,7213
70	112	5,4	78,6	5,4	2,7	163,9344

Table 5.6: Rock sample in nitrogen gas

Time (min)	Total number of counts	% of counts in Window A	% of counts in Window B	% of counts in window C	% of counts in Window D	Rn concentration ($Bq.m^{-3}$)
5	162.	15.4	53.7	22.2	3.1	746.0333
10	253.	8.7	64.8	20.2	1.6	648.7246
15	288.	4.9	61.8	24.0	2.8	324.3623
20	302.	5.0	73.5	12.3	3.0	360.6557
25	296.	5.4	70.3	16.6	2.0	421.671
30	354.	4.2	74.6	13.0	2.6	327.8689
35	340.	5.9	73.0	14.1	2.4	527.4412
40	334.	5.7	69.8	15.9	4.5	395.581
45	297.	5.1	71.7	14.8	2.0	393.4426
50	292.	6.5	79.5	6.5	1.7	524.5901
55	318.	6.3	74.5	11.0	3.8	461.5111
60	286.	5.3	73.4	12.6	2.5	393.4426
65	314.	7.0	77.1	8.9	2.6	593.3713

Table 5.7: Rock sample at 80 kPa.

Time (min)	Total number of counts	% of counts in Window A	% of counts in Window B	% of counts in window C	% of counts in Window D	Rn concentration ($Bq.m^{-3}$)
5	1034.	6.6	77.7	2.4	7.2	1050.462
10	1267.	6.1	81.9	1.4	6.3	1260.821
15	1188.	6.2	80.4	0.9	6.4	1226.745
20	943.	9.2	77.5	2.1	6.5	1920.765
25	727.	7.6	77.6	1.9	8.8	770.7637
30	635.	9.3	72.1	2.1	10.9	861.5874
35	566.	10.6	68.2	2.3	11.5	933.1652
40	527.	10.4	67.6	2.1	14.4	566.5647
45	522.	11.3	68.0	3.8	11.5	966.4926
50	495.	10.9	65.3	3.9	13.7	666.5466
55	532.	13.7	63.9	3.0	13.5	1239.924
60	479.	13.4	62.4	3.1	16.1	866.5106
65	510.	13.3	62.6	2.6	16.3	904.8094
70	484.	14.9	59.5	3.5	18.6	904.8094

Table 5.8: Rock sample experiment of ^{220}Rn emanation at 90 kPa.

Time (min)	Total number of counts	% of counts in Window A	% of counts in Window B	% of counts in window C	% of counts in Window D	Rn concentration ($Bq.m^{-3}$)
5	280.	14.3	71.4	5.7	1.8	1162.176
10	365.	9.3	79.7	3.0	2.2	932.7143
15	414.	9.4	82.6	1.9	1.7	1095.057
20	343.	8.8	79.0	2.3	3.2	760.4562
25	364.	8.0	77.2	3.9	2.5	760.4562
30	366.	9.0	78.2	5.2	2.2	886.9235
35	374.	8.6	77.0	4.0	2.7	825.7563
40	404.	10.9	75.8	3.5	2.7	1205.866
45	402.	10.7	76.4	3.0	3.7	1113.108
50	385.	11.4	75.9	3.9	3.4	1168.526
55	96.	9.4	81.3	1.1	5.2	1010.042

Table 5.9: Rubber sample experiment at 90 kPa.

Time (min)	Total number of counts	% of counts in Window A	% of counts in Window B	% of counts in window C	% of counts in Window D	Rn concentration ($Bq.m^{-3}$)
5	70	7,2	2,9	10	0	13,40162
10	63	6,4	0	7,9	1,6	10,71183
15	72	12,5	4,2	4,2	0	24,10162
20	61	1,7	1,7	3,3	0	3,872331
25	61	6,6	4,9	4,9	3,3	7,748083
30	67	4,5	1,5	9	1,5	10,33078
35	55	9,1	1,8	3,6	0	9,043423
40	56	0	0	8,9	0	6,459588
45	60	0	1,7	5	0	3,874042
50	55	3,6	0	0	0	2,582694
55	53	3,8	0	5,7	0	6,456737
60	54	3,7	0	3,7	0	5,16767
65	63	7,9	3,2	1,6	1,6	6,462442
70	70	1,4	1,4	4,3	0	5,169955
75	55	0	0	0	0	0
80	53	3,8	1,9	3,8	0	5,169955
85	72	8,3	0	2,8	2,8	9,047419
90	60	15	3,3	8,3	1,7	18,09484
95	64	6,3	0	9,4	0	12,92488
100	64	12,5	3,1	1,6	0	11,63754
105	70	4,3	1,4	4,3	1,4	6,462442
110	62	11,3	1,6	8,1	0	15,51672

Table 5.10: Rock sample experiment at 101 kPa.

Time (min)	Total number of counts	% of counts in Window A	% of counts in Window B	% of counts in window C	% of counts in Window D	Rn concentration ($Bq.m^{-3}$)
5	295.	12.9	64.8	7.5	4.4	953.2714
10	423.	11.8	73.1	3.3	6.9	1095.057
15	475.	11.0	73.3	4.6	4.0	1307.985
20	435.	10.8	74.5	4.8	4.2	1168.526
25	439.	6.2	79.3	3.2	4.6	522.7618
30	436.	10.6	77.5	3.9	4.6	1107.025
35	455.	10.6	74.1	3.5	4.4	1174.947
40	424.	11.3	74.3	3.1	5.4	1156.738
45	396.	13.1	70.2	3.8	5.8	1236.786
50	432.	14.1	67.4	3.5	7.0	1422.304